Transport and magnetization dynamics in a superconductor/single-molecule magnet/superconductor junction

S. Teber,[1] C. Holmqvist,[2] and M. Fogelström[2]

[1]*Laboratoire de Physique Théorique et Hautes Energies, Université Pierre et Marie Curie, 4 place Jussieu, 75005 Paris, France*
[2]*Department of Microtechnology and Nanoscience (MC2), Chalmers University of Technology, S-412 96 Göteborg, Sweden*
(Received 20 February 2010; published 4 May 2010)

We study dc-transport and magnetization dynamics in a junction of arbitrary transparency consisting of two spin-singlet superconducting leads connected via a single classical spin precessing at the frequency Ω. The presence of the spin in the junction provides different transmission amplitudes for spin-up and spin-down quasiparticles as well as a time-dependent spin-flip transmission term. For a phase-biased junction, we show that a steady-state superconducting charge current flows through the junction and that an out-of-equilibrium circularly polarized spin current, of frequency Ω, is emitted in the leads. Detailed understanding of the charge and spin currents is obtained in the entire parameter range. In the adiabatic regime, $\hbar\Omega \ll 2\Delta$, where Δ is the superconducting gap, and for high transparencies of the junction, a strong suppression of the current takes place around $\varphi \approx 0$ due to an abrupt change in the occupation of the Andreev bound states. At higher values of the phase and/or precession frequency, extended (quasiparticlelike) states compete with the bound states in order to carry the current. Well below the superconducting transition, these results are shown to be weakly affected by the backaction of the spin current on the dynamics of the precessing spin. Indeed, we show that the Gilbert damping due to the quasiparticle spin current is strongly suppressed at low temperatures, which goes along with a shift of the precession frequency due to the condensate. The results obtained may be of interest for ongoing experiments in the field of molecular spintronics.

I. INTRODUCTION

Spintronics exploits the fact that an electron current consists of spinful carriers, with information stored in their spin state, which interact in a controlled way with their magnetic environment. Research in this field was pioneered in 1970 with the experiments of Tedrow and Meservey[1] on ferromagnet/superconductor tunnel junctions as well as the experiments of Jullière[2] on magnetic tunnel junctions. It fully emerged in 1980 with the observation of spin-polarized electron injection from a ferromagnetic metal to a normal metal[3] followed by the discovery of the well-known giant magnetoresistance (GMR) effect.[4,5] Since then, most of the studies focused on stationary magnetic states and the control of the electrical current by tuning the state of the magnet as in, e.g., GMR, see Ref. 6 for a review. The study of the magnetization dynamics in ferromagnet (F)/normal (N) metal as well as F/superconductor (S) hybrids is much more recent and basically involves controlling the state of the magnet with the help of an applied electrical current. The main trigger was the experimental confirmation of the ideas of Slonczewski[7] and Berger[8] that an electrical current may affect the state of the magnet via a spin-transfer torque, see Ref. 9 for a pedagogical introduction. Indeed, a spin-polarized current of high enough density injected into a ferromagnet was shown to reverse the magnetization or generate a steady-state precessing magnetization in accordance with theoretical predictions. Many recent experiments have confirmed these facts, see Ref. 10 for a review. Conversely, a microwave-driven precessing magnetization of a ferromagnetic layer under ferromagnetic resonance (FMR) was shown to emit pure spin currents, i.e., without any associated net charge transfer, into the adjacent normal-metal layers, see

Refs. 11 and 12 for the theory. Such a spin current was only indirectly measured as an enhancement of the Gilbert damping of the magnetization dynamics.[13] Recently, a similar experiment has been performed on S/F hybrids.[14] Contrary to the case of N/F hybrids, it was shown that the Gilbert damping is reduced at temperatures well below the superconducting transition temperature, see Ref. 15 for the theory.

At the same time, there is a fast growing interest in controlling the spin orientation of single molecules or even a single or a few atoms in order to perform basic quantum operations. Recently, the control of the spin orientation of a single manganese atom in a semiconductor quantum dot could be achieved with the help of optical techniques.[16] At the molecular level, the experimental challenge is already at the level of designing a molecular junction. Single-molecule magnets (SMMs) were recently contacted to metallic leads allowing electron-transport measurement through them[17,18] to probe their properties, see Refs. 19 and 20 for recent reviews on SMMs. The access resistance due to the normal contacts may however be a source of limitation which motivated the design of superconducting molecular junctions. This was first done with semiconducting nanowires,[21] carbon nanotubes,[22–25] and more recently with a single C_{60} fullerene molecule.[26] Magnetically active metallofullerene molecules could also be contacted to superconducting leads and the proximity-induced superconductivity was studied via low-temperature transport measurements.[27] On the theoretical side, equilibrium properties of such Josephson junctions were extensively studied since a long time, see Refs. 28–33 without being extensive; the effect of magnetization dynamics has been discussed more recently, see, e.g., Refs. 34–38.

Motivated by the recent experimental breakthroughs of molecular spintronics we study, in the present paper, a
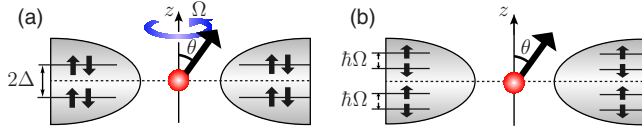
FIG. 1. (Color online) Schematic representation of a localized spin (red dot) contacted to superconducting leads representing a short S/SMM/S junction (S is for superconductor and SMM for single-molecule magnet). (a) In the laboratory frame, the spin is precessing and the leads are spin degenerate. (b) In the rotating frame, the tilted spin is static and an effective magnetic field, $h_z = \Omega/2$, lifts the spin degeneracy as well as modifies the occupation functions of the particles in the leads.

model, first proposed in Refs. 34 and 35, describing a short (shorter than the superconducting coherence length) clean junction consisting of a single precessing spin, with precession frequency Ω, connected to spin-singlet superconducting BCS leads, see Fig. 1(a). The precessing spin provides different transmission probabilities for spin-up and spin-down quasiparticles. It is assumed to be the one of, e.g., a molecular magnet. The latter have a total spin of quite large magnitude, e.g., $S = 10$ for Fe_8 in its ground state. For simplicity, we will neglect its quantum fluctuations and consider that this spin is classical. On the basis of such a model, our goal will be to compute the dc-transport properties of the junction. With respect to Refs. 34 and 35, we will consider a junction of arbitrary transparency and, besides the dc charge current, we will also compute the dc spin current across the junction. Even though such a setup is still challenging to realize experimentally the corresponding simplified model constitutes an interesting theoretical playground in order to study the combined effects of both superconductivity and magnetization dynamics at the molecular scale.

Magnetization dynamics drives the system out of equilibrium. This can be most easily seen by going to the rotating frame, Fig. 1(b), where the tilted molecular spin is static and an effective z-directed magnetic field, $h_z = \Omega/2$, acts on the leads. Contrary to a usual magnetic field, see, e.g., Ref. 39, and references therein, we will show in the following that h_z affects the occupation functions of the leads translating the out-of-equilibrium nature of the problem. In the case of normal leads, no dc charge current can flow through the junction. Nevertheless, the nonequilibrium spin accumulation, i.e., the difference in chemical potential, $\hbar\Omega$ at $T = 0$, between spin-up and spin-down quasiparticles, drives the emission of a spin current in the leads. In analogy with the case of the macromagnet mentioned above, this spin current will in turn damp the precession of the molecular spin eventually leading to its complete alignment with the external applied magnetic field.

Combining these out-of-equilibrium effects with superconductivity in the leads brings interesting features, even in the dc case.40 Indeed, integrating the junction into a superconducting loop yields a superconducting phase difference between the leads, $\varphi = -2\pi\Phi/\Phi_0$, where Φ is the total magnetic flux across the loop and $\Phi_0 = h/2e$ is the magnetic-flux quantum. Cooper pairs may then be transferred across this phase biased junction leading to the dc Josephson effect. Microscopically, this transfer relies on the existence of An-

dreev bound states.42 The phase dependence of the current is directly related to the phase dependence of the spectrum of these subgap states. In the case of a tunnel junction, without any magnetic impurity, the current-phase relation (CPR) follows the well-known sinusoidal relation $I^c(\varphi) = I_C \sin\varphi$, where I_C is the critical current depending on the normal resistance of the junction. In more complex cases, significant departures from this sinusoidal relation are known to take place, see Ref. 43 for a review. One well-known origin for such a departure is the increase in the transparency, $\mathcal{T}$, of the junction leading to phase-coherent transfer of multiple Cooper pairs across the junction. In the ballistic limit, $\mathcal{T} = 1$, and at low temperatures $(T) : I^c(\varphi) \propto \sin(\varphi/2)$. Another known source of departure originates from preparing the system in an out-of-equilibrium state, e.g., such as by a microwave irradiation of the junction, see Refs. 44 and 45 for recent experiments and Ref. 46 for the theory. In the present problem, both of the these features are present. We will show that they strongly affect the CPR in a way which is proper to the (time-dependent) magnetic interface we consider. Concerning the out-of-equilibrium spin current we will show, in accordance with the case of the macromagnet considered above, that it is strongly reduced deep in the superconducting phase. This will in turn suppress the damping of the precession providing a self-consistent check of the robustness of the transport properties of the junction. The remaining superconducting part of the spin current will also be shown to shift the precession frequency.

The paper is organized as follows. In Sec. II, we present the model34,35 of a Josephson junction with a precessing spin. In Sec. III, we solve this model analytically, in the tunnel limit and zero temperature, to understand the basic physics of the problem. In order to deal with a junction of arbitrary transparency we present, in Sec. IV, a resummation method37 based on a usual Green's-function approach combined with a unitary transformation to the rotated frame. This method provides a convenient interpretation of the out-of-equilibrium features of the system. It is also simple to implement numerically. In Secs. V and VI, the combined analytical and numerical results, for arbitrary transparency and finite temperatures, are presented and discussed for the charge and spin currents, respectively. Finally in Sec. VII, we summarize our results and conclude. In the following $\hbar = k_B = 1$ everywhere unless specified.

II. MODEL

The model we shall consider is based on the following time-dependent tunnel junction Hamiltonian:34,35

$$H(t) = H_L + H_R + H_T(t), \tag{1}$$

where the perturbation-theory series for the time-dependent perturbation, H_T, will be summed to infinite order in what follows. In Eq. (1), the first two terms correspond to the Hamiltonians of the right (R) and left (L) spin-singlet BCS superconducting leads,

$$H_\alpha = \sum_{\mathbf{k},\sigma} \xi_{\mathbf{k}} c^\dagger_{\alpha,\mathbf{k},\sigma} c_{\alpha,\mathbf{k},\sigma} + \sum_{\mathbf{k}} [\Delta_\alpha c^\dagger_{\alpha,\mathbf{k},\uparrow} c^\dagger_{\alpha,-\mathbf{k},\downarrow} + \text{H.c.}], \quad (2)$$

where $\xi_{\mathbf{k}}$ is the single-particle spectrum, the (temperature-dependent) gap is given by $\Delta_\alpha = \Delta(T) e^{i\chi_\alpha}$ and χ_α is the superconducting phase in lead $\alpha = R, L$. The last term in Eq. (1) corresponds to the tunneling Hamiltonian between the leads,

$$H_T(t) = \sum_{\mathbf{k},\mathbf{q},\sigma,\sigma'} [c^\dagger_{R,\mathbf{k},\sigma} T_{\sigma,\sigma'}(t) c_{L,\mathbf{q},\sigma'} + \text{H.c.}] \quad (3)$$

with a time-dependent transmission amplitude reading

$$T(t) = T_0 \mathbf{1}_2 + T_1 \mathbf{S}(t) \cdot \vec{\sigma}, \quad (4)$$

where $\mathbf{1}_2$ is the unit 2×2 matrix and $\vec{\sigma} = (\sigma_x, \sigma_y, \sigma_z)$ is the vector of Pauli spin matrices. The time dependence in Eq. (4) originates from the precessing motion of the classical spin localized in the junction. The corresponding classical equation of motion reads

$$\partial_t \mathbf{S} = -\gamma \mathbf{S} \times \mathbf{H}_{eff}, \quad (5)$$

where γ is the gyromagnetic ratio and $\mathbf{H}_{eff} = H_{eff}\hat{z}$ is an effective z-directed magnetic field including the applied field as well as other contributions such as crystal anisotropy and demagnetization fields. The solution to Eq. (5) reads

$$\mathbf{S}(t) = S(\sin\theta\cos\Omega t, \sin\theta\sin\Omega t, \cos\theta), \quad (6)$$

where θ is the tilt angle of the spin with respect to the z axis and $\Omega = \gamma H_{eff}$ the precession frequency around this axis.

In spin space, the transmission amplitude matrix reads

$$T(t) = T_0 \mathbf{1}_2 + T_\| \sigma_z + T_\perp \sigma_x e^{-i\sigma_z \Omega t}, \quad (7)$$

where T_0 is the direct transmission amplitude whereas $T_\| = T_1 S_z$ and $T_\perp = T_1 S_\perp$ are the spin-conserving and spin-flip transmission amplitudes, respectively. The latter two depend on the magnitude, S, of the spin localized in the junction as well as on its orientation, θ, with respect to the quantization axis,

$$T_\| = T_S \cos\theta, \quad T_\perp = T_S \sin\theta, \quad T_S = T_1 S. \quad (8)$$

In the absence of precession, $\Omega = 0$, and for normal metallic leads, the model in Eq. (1) was first proposed by Appelbaum[28] in order to explain tunnel conductance anomalies due to magnetic impurities. Its microscopic justification was provided by Anderson[29] who has shown, on the basis of the Schrieffer-Wolff transformation, that

$$T_1 = 2V^2_{mix} \frac{U}{\epsilon_d(\epsilon_d + U)}, \quad (9)$$

where V_{mix} mixes the spin states of the conduction electrons with the one of the localized spin in the junction, $\epsilon_d < 0$ is the energy of an electron on the localized state and $\epsilon_d + U$ that to add a second one taking into account of the Coulomb charging energy U. If either ϵ_d or $\epsilon_d + U$ are close to the Fermi level, tunneling through the magnetic impurity will dominate direct tunneling, i.e., $T_1 \gg T_0$. In the case of a superconducting junction, still with $\Omega = 0$, the model was first considered by Kulik[30] and Bulaevskii *et al.*[31] for an ensemble of impurities in the dielectric layer between the superconductors. In

the lowest order of perturbation theory, they have shown that, in the case where $T_S > T_0$, the junction is in a π state. Recently, the model was reconsidered by Zhu and Balatsky[34] for a single classical precessing spin in the junction. At the lowest order in perturbation theory, they have shown that the dc Josephson current is not modulated in time by the precession of the spin. Latter studies have focused on the backaction of the current on the precessing spin showing a possible nutation.[35]

We reconsider here the model of a single classical precessing spin in a superconducting junction keeping in mind that the single spin may correspond to, e.g., an SMM such as Mn_{12} or Fe_8. The latter have large S which should favor the tunneling through the spin, $T_S > T_1$. Moreover, at the molecular level, one may expect that the tilt angle θ may be varied in a larger range than for a ferromagnet under FMR.[41] The cases where either $T_\| \ll T_\perp$ (large tilt angles) or $T_\| \gg T_\perp$ (small tilt angles) will therefore be considered in the following.

As stated in Sec. I, our goal is to explore the transport properties of such a superconducting junction: charge as well as spin currents, for a single conducting channel, arbitrary transparency and temperatures below the superconducting critical temperature.

III. TUNNEL LIMIT

In this section, we consider the simple limit of a tunnel junction. The results obtained in this limit allow for a direct understanding of the basic influence of the precessing spin on the current flowing through the junction as well as the basic backaction of the (spin) current on the magnetization dynamics.

A. Charge current

In the tunnel limit, the current at lead $\alpha = R, L$ may formally be separated into normal an anomalous contributions,

$$I^c_\alpha(t) = I^c_{\alpha,G}(t) + I^c_{\alpha,F}(t), \quad (10a)$$

$$I^c_{\alpha,G}(t) = -e \int_{-\infty}^t dt' [\langle [A^c_\alpha(t), A^{c\dagger}_\alpha(t')] \rangle + \text{H.c.}], \quad (10b)$$

$$I^c_{\alpha,F}(t) = -e \int_{-\infty}^t dt' [\langle [A^c_\alpha(t), A^c_\alpha(t')] \rangle + \text{H.c.}], \quad (10c)$$

where $I^c_{\alpha,G}$ is the normal contribution to the charge current and $I^c_{\alpha,F}$ the anomalous one. In the following, we will compute the current at the left lead ($\alpha = L$). The current at the right lead follows from charge conservation, $I^c_R = -I^c_L$ so that in the rest of this section, we will drop the lead index. In the interaction representation, the operator, $A^c_L \equiv A^c$, appearing in Eq. (10), is defined as[47]

$$A^c(t) = \sum_{\mathbf{k},\mathbf{p},\sigma,\sigma'} c^\dagger_{R,\mathbf{k},\sigma}(t) T_{\sigma,\sigma'}(t) c_{L,\mathbf{p},\sigma'}(t) \quad (11)$$

and depends on the spin- and time-dependent tunneling amplitudes which were defined in Eq. (7) and below. For a

spin-singlet superconducting junction, the dc charge current is time independent[34] and, in what follows, we shall focus on its precession-frequency dependence.

In the absence of applied bias, $I_G^c = 0$, and only the anomalous part contributes to the total dc current. The latter reads

$$I_G^c = 4e[(T_0^2 - T_\parallel^2)\text{Re }\mathcal{D}^R(0) - T_\perp^2 \text{ Re }\mathcal{D}^R(\Omega)]\sin\varphi, \quad (12)$$

where $\varphi = \chi_R - \chi_L$, the total phase difference across the junction, was gauged out from the gap so that $\Delta_\alpha = \Delta$ is real. The charge current of Eq. (12) depends on the reactive part of the anomalous two-particle propagator defined (in imaginary time) as

$$\mathcal{D}(i\omega) = \sum_{\mathbf{k},\mathbf{q}} \frac{1}{\beta} \sum_{i\epsilon} \mathcal{F}_R^\dagger(\mathbf{k},i\epsilon)\mathcal{F}_L(\mathbf{q},i\epsilon - i\omega) \quad (13)$$

from which the retarded and advanced functions are obtained by an analytic continuation, $i\omega \to \omega \pm i\eta$ ($\eta = 0^+$), respectively. The Matsubara superconducting Green's functions are defined in the usual way:[47] $\mathcal{G}_\alpha$ is the normal component and $\mathcal{F}_\alpha = \mathcal{F}_\alpha^\dagger$ ($\Delta \in \mathbb{R}$) are the anomalous components of the Green's function in lead α. In the following, we will mainly work with quasiclassical Green's functions that we simply define as $g_\alpha = \Sigma_\mathbf{k}\mathcal{G}_{\alpha,\mathbf{k}}$, $f_\alpha = f_\alpha^\dagger = \Sigma_\mathbf{k}\mathcal{F}_{\alpha,\mathbf{k}}$. For noninteracting leads, they read

$$g_\alpha^{(0)}(i\epsilon) = -\pi\nu_N \frac{i\epsilon}{\sqrt{\epsilon^2 + \Delta^2}}, \quad f_\alpha^{(0)}(i\epsilon) = \pi\nu_N \frac{\Delta}{\sqrt{\epsilon^2 + \Delta^2}}, \quad (14)$$

where the single-particle spectrum of the electrons in the leads has been linearized around the Fermi surface, ν_N is the normal-state density of states (DOS), and $\Delta \equiv \Delta(T)$ is temperature dependent. With the help of Eq. (14), Eq. (13) reads

$$\mathcal{D}(i\omega) = \pi^2\nu_N^2\Delta^2 \frac{1}{\beta} \sum_{i\nu} \frac{1}{\sqrt{[\nu^2 + \Delta^2][(\nu+\omega)^2 + \Delta^2]}},$$

where the integrand[48] is a pure branch cut. This is a consequence of the singular BCS density of states at the gap edges. These gap-edge singularities will affect the response function, a signature of the fact that extended states contribute to the current. As a result, the supercurrent will have a nonanalytic dependence on the precession frequency. This can readily be seen from the zero-temperature ($T = 0$) expression of the propagator (the reactive part being even and the dissipative part odd with respect to x we only consider $x > 0$ in what follows),

$$\text{Re }\mathcal{D}^R(x) = \begin{cases} \pi\nu_N^2\Delta K(x), & x < 1 \\ \pi\nu_N^2\dfrac{\Delta}{x}K\left(\dfrac{1}{x}\right), & x > 1, \end{cases} \quad (15a)$$

$$\text{Im }\mathcal{D}^R(x) = \frac{\pi\nu_N^2\Delta}{x+1}K\left(\frac{x-1}{x+1}\right)\Theta(x-1), \quad (15b)$$

where $x = \omega/2\Delta$, K is the complete elliptic integral of the first kind, and Θ is the Heaviside function. The elliptic integral is logarithmically singular for $\omega = 2\Delta$ which, by Kramers-Kronig, is related to the finite jump of Im $\mathcal{D}^R$ at this fre-
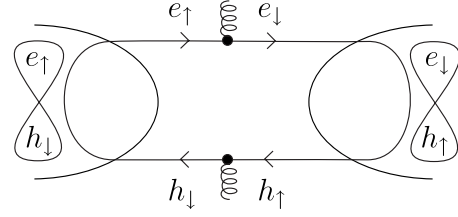

FIG. 2. Lowest-order diagram for the Josephson current showing the transfer of a Cooper pair from one lead to the other. The curvy lines correspond to the absorption/emission of a quantum of precession ($\hbar\Omega$) while e_σ and h_σ denote particles and holes of spin σ, respectively. This diagram shows that the Josephson current is of second order in $\Omega/2\Delta$.

quency. With the help of Eqs. (12) and (15a), the charge current reads

$$I^c = \begin{cases} 2e\Delta\left[(t_0^2 - t_\parallel^2) - t_\perp^2\dfrac{2}{\pi}K\left(\dfrac{\Omega}{2\Delta}\right)\right]\sin\varphi, & \Omega < 2\Delta, \\[3mm] 2e\Delta\left[(t_0^2 - t_\parallel^2) - t_\perp^2\dfrac{4\Delta}{\pi\Omega}K\left(\dfrac{\Omega}{2\Delta}\right)\right]\sin\varphi, & \Omega > 2\Delta, \end{cases}$$

$$(16)$$

where reduced hopping amplitudes have been introduced, $t_i = T_i/W$ ($W = 1/\pi\nu_N$ is the bandwidth).

As first noticed by Kulik[30] and Bulaevskii *et al.*,[31] for a static spin, the results of Eq. (16) first show that the presence of the spin in the junction reduces the current. As will be shown by a calculation to all orders in the tunnel amplitude, in Sec. V, a crossover to a π junction indeed takes place when the spinconserving, $t_\parallel$, and/or spin-flip, $t_\perp$, tunnel amplitudes become on the order of the amplitude, t_0, for direct tunneling.

Moreover, at zero precession frequency, the current due to t_0 or $t_\parallel$ and $t_\perp$ corresponds to the usual tunnel limit of the Josephson current for a 0 or π junction, respectively. The situation becomes more interesting when the system is driven out of equilibrium by the external classical source and the spin in the junction precesses. As can be seen from Eq. (16), the precession-frequency-dependent part of the supercurrent is entirely carried by the spin-flip term. In order to single out this contribution, we will therefore focus, in what follows, on $\delta I^c = I^c(\Omega) - I^c(0)$.

At low frequencies, $\Omega < 2\Delta$, the charge current increases with increasing precession frequency (recall that $\Omega > 0$). In particular, in the adiabatic limit ($\Omega \ll 2\Delta$), the supercurrent arising from spin flips reads

$$\delta I^c \approx -\frac{et_\perp^2\Delta}{2}\left(\frac{\Omega}{2\Delta}\right)^2\sin\varphi, \quad \Omega \ll 2\Delta, \quad (17)$$

where the lowest-order term is of second order in the precession frequency. This comes from the two-particle nature of the Josephson current, see Fig. 2. Indeed, in order to transfer a Cooper pair from one lead to another, an Andreev spin-down/spin-up electron together with its retroreflected spin-up/spin-down hole will flip their spins absorbing/emitting a quantum of precession. The spin-up band is therefore sepa-

rated from the spin-down one by an energy interval equal to Ω. As will be shown in more details in Sec. IV A, $\Omega/2$ corresponds to an effective z-directed magnetic field applied to the leads. This agrees with interpreting Ω as a Zeeman splitting between the spin bands, see Fig. 1(b).

On the other hand, at high frequencies, $\Omega \gg 2\Delta$, the supercurrent arising from spin-flip processes decreases,

$$\delta I^c \approx -2et_\perp \Delta \frac{2\Delta}{\Omega} \sin \varphi, \quad \Omega \gg 2\Delta. \quad (18)$$

Finally, in the intermediate range, a resonance appears at $\Omega = 2\Delta$ where the spin-flip supercurrent diverges logarithmically,

$$\delta I^c \approx \frac{2et_\perp^2}{\pi} \Delta \log\left(\left|\frac{\Omega}{2\Delta} - 1\right|\right) \sin \varphi, \quad \Omega \approx 2\Delta. \quad (19)$$

Following the discussion at the level of the two-particle propagator, such a singularity translates the fact that, when the system is driven at the frequency 2Δ by the external source, an infinite number of extended states are available to carry the current.[50]

The regime in which Eqs. (18) and (19) are valid requires high precession frequencies, at least on the order of the amplitude of the superconducting gap. It may be difficult to reach, by an order of magnitude, in practice and would lead to a heating up of the system as witnessed by the fact that transport in this regime is dominated by extended states. In the following, we will therefore be mainly interested in the adiabatic regime where $\Omega \ll 2\Delta$, and the electronic degrees of freedom (of time scale $\hbar/\Delta$) adjust instantaneously to the magnetic ones (of time scale $2\pi/\Omega$).

B. Spin current

The spin current at a given lead[52] can be calculated along the same lines as the charge current (recall that $\hbar = 1$ unless specified),

$$\mathbf{I}^s(t) = \mathbf{I}_G^s(t) + \mathbf{I}_F^s(t), \quad (20a)$$

$$\mathbf{I}_G^s(t) = \frac{1}{2} \int_{-\infty}^t dt' [\langle [\mathbf{A}^s(t), A^{c\dagger}(t')] \rangle + \text{H.c.}], \quad (20b)$$

$$\mathbf{I}_F^s(t) = \frac{1}{2} \int_{-\infty}^t dt' [\langle [\mathbf{A}^s(t), A^c(t')] \rangle + \text{H.c.}], \quad (20c)$$

where $\mathbf{I}_G^s$ is the normal contribution to the spin current and $\mathbf{I}_F^s$ the anomalous one. Contrary to the case of the charge current, there is no conservation law related to the spin of the electrons in the leads. Rather than transferring spins from one lead to the other, the precessing single-molecule magnet ejects spins in a symmetric way in the two leads ($\mathbf{I}_R^s = \mathbf{I}_L^s$), see Ref. 10 where this point was emphasized. Therefore, there is no global spin current flowing through the junction. In Eq. (20), the operator A^c is the one which was defined in Eq. (11) and, still in the interaction representation, the operator $\mathbf{A}^s$ is defined as

$$\mathbf{A}^s(t) = \sum_{\mathbf{k},\mathbf{p},\sigma,\sigma',\sigma''} c_{R,\mathbf{k},\sigma}^\dagger(t) \vec{\sigma}_{\sigma,\sigma'} T_{\sigma',\sigma''}(t) c_{L,\mathbf{p},\sigma''}(t). \quad (21)$$

Both the normal and anomalous parts contribute to the total dc spin current which reads

$$I_z^s = 2T_\perp^2 [\text{Im } \mathcal{D}^R(\Omega)\cos \varphi - \text{Im } \mathcal{Q}^R(\Omega)], \quad (22a)$$

$$\begin{aligned} I_x^s = {} & 2T_\parallel T_\perp \{\text{Im } \mathcal{Q}^R(\Omega)\cos(\Omega t) \\ & - [\text{Re } \mathcal{Q}^R(\Omega) - \text{Re } \mathcal{Q}^R(0)]\sin(\Omega t)\} \\ & + 2T_0 T_\perp \{\text{Im } \mathcal{D}^R(\Omega)\sin(\Omega t) \\ & + [\text{Re } \mathcal{D}^R(\Omega) - \text{Re } \mathcal{D}^R(0)]\cos(\Omega t)\}\sin \varphi \\ & + 2T_\parallel T_\perp \{\text{Im } \mathcal{D}^R(\Omega)\cos(\Omega t) - [\text{Re } \mathcal{D}^R(\Omega) \\ & - \text{Re } \mathcal{D}^R(0)]\sin(\Omega t)\}\cos \varphi \end{aligned} \quad (22b)$$

and the y component is derived from the x component with the help of the substitution, $\Omega t \to \Omega t - \pi/2$, in I_x^s. This general result shows that the precession of the spin in the junction transfers spins into the adjacent leads (see below for the difference between normal and superconducting leads). Moreover, Eq. (22b) shows that, contrary to the charge current, the spin current is circularly polarized in the xy plane and rotates in time at the precession frequency of the spin localized in the junction. Finally, the expression of the spin current involves not only the reactive part of the anomalous propagator but also its dissipative part. This is related to the fact that the spin current arises from breaking singlet pairs. Concomitantly, the normal part also contributes to the spin current and is associated with $\mathcal{Q}$, the normal two-particle propagator, defined (in imaginary time) as

$$\mathcal{Q}(i\omega) = \sum_{\mathbf{k},\mathbf{q}} \frac{1}{\beta} \sum_{i\epsilon} \mathcal{G}_R(\mathbf{k}, i\epsilon - i\omega)\mathcal{G}_L(\mathbf{q}, i\epsilon), \quad (23)$$

where $\mathcal{G}$ is the normal component of the superconducting Green's function and the expression of the related noninteracting quasiclassical function has been given in Eq. (14). With the help of this equation, and at zero temperature, a direct computation of Eq. (23) yields ($x > 0$),

$$\text{Re } \mathcal{Q}^R(x) = \text{Re } \mathcal{Q}^R(0) - \pi \nu_N^2 \Delta q(x), \quad (24a)$$

$$\begin{aligned} \text{Im } \mathcal{Q}^R(x) = {} & -\frac{2\pi \nu_N^2 \Delta}{1+x}\left[K\left(\frac{x-1}{x+1}\right) + (x^2 - 1)E\left(\frac{x-1}{x+1}\right)\right] \\ & \times \Theta(x-1), \end{aligned} \quad (24b)$$

where $x = \omega/2\Delta$, K and E are the complete elliptic integrals of the first and second kinds, respectively, and Θ is the Heaviside function. Notice that, in Eq. (24a), the combination $\text{Re } \mathcal{Q}^R(x) - \text{Re } \mathcal{Q}^R(0)$ eliminates an ultraviolet singularity in the propagator. The remaining function $q(x)$ is smooth and $q(x) \to 0$ in the limit $x \to \infty$ (i.e., where $\Delta \to 0$) while $q(x) \to 3\pi x^2/8$ in the limit $x \to 0$. Because the imaginary part has a finite jump at $x = 1$, the real part diverges logarithmically at this point. The fact that the normal component enters the expression of the spin current allows us to consider both cases of normal and superconducting leads.
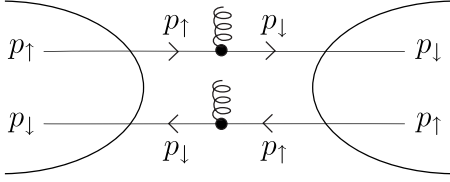
FIG. 3. Lowest-order diagram for the normal spin current showing the transfer of quasiparticles of spin σ, denoted as p_σ. The curvy lines correspond to the emission/absorption of a quantum of precession. This diagram shows that the normal spin current is of first order in $\Omega/2\Delta$ and that it is symmetric between the two leads.

1. Normal leads

Being particularly simple, the case of normal leads where $\Delta=0$ is worth examining. In this case, the $T=0$ spin current arises solely from quasiparticles and reads

$$I_z^s = \frac{2t_\perp^2}{\pi}\Omega, \tag{25a}$$

$$I_x^s = -\frac{2t_\parallel t_\perp}{\pi}\Omega\cos(\Omega t), \tag{25b}$$

$$I_y^s = -\frac{2t_\parallel t_\perp}{\pi}\Omega\sin(\Omega t). \tag{25c}$$

This equation can be written in a more compact form as

$$\mathbf{I}^s = \frac{2t_S^2}{\pi S^2}\mathbf{S}\times\partial_t\mathbf{S}, \tag{26}$$

where Eqs. (5), (6), and (8) have been used and the reduced hopping amplitude through the spin has been introduced, $t_S = T_S/W$ ($W=1/\pi\nu_N$ is the bandwidth). Equations (25b) and (25c) explicitly show the circular polarization of the spin current in the xy plane. The x and y components of the average number of spins,

$$\langle I_j^s\rangle = \int_0^{2\pi/\Omega}\frac{dt}{2\pi}I_j^s(t), \tag{27}$$

where $j=x,y$, emitted in the leads is zero. On the other hand, the z component of the spin current is time independent and has a linear dependence on the precession frequency. From Eq. (27), we see that $\langle I_z^s\rangle=4t_S^2$. As schematically represented in Fig. 3, this transfer of spin is symmetric between the two leads and we have $I_\uparrow^c = -I_\downarrow^c$, which confirms the fact that there is a nonzero z component of the spin current and no associated charge current. These arguments show that the normal junction is a pure spin pump where the two periodic parameters are the projections of the in-plane spin along the x and y axes, see Ref. 53 in the case of a quantum dot as well as Ref. 10 where similar results are reviewed in the case of an F/N junction. The linearity of the spin current with respect to the precession frequency is related to the single-particle nature of the tunneling quasiparticles.

2. Superconducting leads

The N/SMM/N case considered in the previous paragraph may formally correspond to the S/SMM/S case in the limit where $\Omega\gg2\Delta\to0$, and extended (quasiparticlelike) states carry all the current. In the opposite regime of low-precession frequencies, $\Omega\ll2\Delta$, the dissipative part of the propagator vanishes suggesting that the (spin-singlet) condensate plays a dominant role. Nevertheless, we still get a nonzero spin current arising from the reactive part of the normal as well as anomalous propagators. With the help of Eqs. (22) and (24)), the $T=0$ dc spin current reads

$$I_z^s = 0, \tag{28a}$$

$$\begin{aligned}I_x^s = &\frac{t_0 t_\perp\Delta}{4}\left(\frac{\Omega}{2\Delta}\right)^2\cos(\Omega t)\sin\varphi\\&+\frac{t_\parallel t_\perp\Delta}{4}\left(\frac{\Omega}{2\Delta}\right)^2(3-\cos\varphi)\sin(\Omega t),\end{aligned} \tag{28b}$$

$$\begin{aligned}I_y^s = &\frac{t_0 t_\perp\Delta}{4}\left(\frac{\Omega}{2\Delta}\right)^2\sin(\Omega t)\sin\varphi\\&-\frac{t_\parallel t_\perp\Delta}{4}\left(\frac{\Omega}{2\Delta}\right)^2(3-\cos\varphi)\cos(\Omega t).\end{aligned} \tag{28d}$$

These equations show that, in analogy with the charge superconducting current, the spin current depends on the superconducting phase difference and has a quadratic dependence on the precession frequency at low frequencies. This suggests that this spin current is of superconducting nature, i.e., related to the tunneling of pairs of particles. Its quadratic dependence on the precession frequency implies that it is smaller than the quasiparticle spin current by a factor on the order of Ω/Δ, i.e., at least one order of magnitude in the adiabatic regime. Actually, because of the singlet nature of the pairs the average number of spins emitted in the leads, $\langle I_j^s\rangle=0$ for $j=x,y,z$, as can be seen with the help of Eqs. (27) and (28). Moreover, its phase dependence shows that the spin current in the case of a π junction is twice larger than in the case of a 0 junction. In these two cases, the expression of the spin current slightly simplifies and its time dependence is seen to be out of phase with respect to the one of the quasiparticle spin current of Eq. (25) by 90°. It can be written in a more compact form as

$$\mathbf{I}^s(\varphi) = \mathcal{N}_\varphi\frac{t_S^2}{4S^2}\frac{\gamma\mathbf{S}\cdot\mathbf{H}_{eff}}{2\Delta}\gamma\mathbf{S}\times\mathbf{H}_{eff}, \tag{29}$$

where $\mathcal{N}_0=1$ and $\mathcal{N}_\pi=2$, for $\varphi=0$ and $\varphi=\pi$, respectively.

C. Gilbert damping

In the last paragraph, we have shown that a precessing molecular spin transfers a spin current to its environment (either metallic or superconducting leads), even if no voltage bias is applied. Following Sec. I, the emission of a spin current by the precessing spin in the junction implies in turn that it is loosing angular momentum. The corresponding spin-transfer torque[7] is given by

$$\vec{\tau}^s = \mathbf{I}_L^s - \mathbf{I}_R^s = 2\mathbf{I}_L^s \tag{30}$$

and has to be added as a source of damping into the classical equations of motion of the precessing spin,

$$\partial_t \mathbf{S} = -\gamma \mathbf{S} \times \mathbf{H}_{eff} + \vec{\tau}^s. \tag{31}$$

If the external source does not compensate for this loss, the damping of the precession will lead to a complete alignment of the spin with the applied magnetic field.

In the case of normal leads, we see from Eq. (26) that the spin-transfer torque corresponds to a Gilbert term leading indeed to a damping of the precession. The corresponding Gilbert constant, at $T=0$, has the following expression:

$$\alpha_S = \frac{4t_S^2}{\pi}, \tag{32}$$

and only depends on the transparency of the junction. On the other hand, in the case of superconducting leads with $\varphi = 0$ or π, Eq. (29) shows that the damping is suppressed and that the superconducting spin current only leads to a shift of the precession frequency,

$$\Omega' = \Omega \left[1 - \frac{\zeta_S}{S} \right], \tag{33}$$

where, at $T=0$, ζ_S reads

$$\zeta_S = \mathcal{N}_\varphi \frac{t_S^2}{2} \frac{\Omega}{2\Delta} \cos \theta. \tag{34}$$

Equation (34) shows that the shift of the precession frequency depends on the precession frequency itself as well as on the tilt angle of the precessing spin and the superconducting phase.

In agreement with the results of the previous paragraph, we arrive at the conclusion that a spin precessing between superconducting leads is only weakly perturbed by its environment with respect to a spin precessing between normal metallic leads. Uniting these two descriptions within a common framework, based on the two-fluid model, this dramatic reduction in the dissipation is natural since quasiparticles are frozen deep in the superconducting state and that the main current carriers are spin singlets.

IV. GENERAL TRANSPORT EQUATIONS

In order to go beyond the tunnel limit, we present in this section a unitary transformation which relates the time-dependent problem to a time-independent one with noncolinear magnetization. This will allow us to reduce the Dyson equations for the dressed Green's function to a set of algebraic equations. In particular, an explicit expression for the Keldysh Green's function can be obtained from which the charge and spin currents may easily be computed, at least numerically.

A. Unitary transformation

In order to take into account of both spin-flip processes and superconductivity in a compact way, we consider a space

which is the tensor product of spin and Gorkov-Nambu spaces, denoted as spin $\otimes$ Nambu in what follows. In this four-dimensional space, we introduce the following bispinor,

$$\hat{\psi}_{\alpha,\mathbf{k}}^\dagger = (c_{\alpha,\mathbf{k},\uparrow}^\dagger, c_{\alpha,\mathbf{k},\downarrow}^\dagger, c_{\alpha,-\mathbf{k},\uparrow}, c_{\alpha,-\mathbf{k},\downarrow}), \tag{35}$$

where the hat denotes operators acting in spin $\otimes$ Nambu space. For example, the spin and Nambu Pauli matrices, $\hat{\sigma}$ and $\hat{\tau}$, respectively, acting on the bispinor of Eq. (35) are defined as

$$\hat{\sigma}_i = \begin{pmatrix} \sigma_i & 0 \\ 0 & -\sigma_i \end{pmatrix}, \quad \hat{\tau}_i = \begin{pmatrix} 0 & \sigma_i \\ -\sigma_i & 0 \end{pmatrix}, \tag{36}$$

where $i=0,1,2,3$ and $\sigma_0 = \mathbf{1}_2$ while the 1,2,3 components of σ_i correspond to the usual x,y,z matrices, respectively.

With these conventions in hand, the action associated with the Hamiltonian in Eq. (1) and evaluated along an arbitrary (for the moment) $\mathcal{C}$ contour reads

$$S[\hat{\psi}, \hat{\psi}^\dagger] = \int_{\mathcal{C}} dt \left[\sum_{\alpha,\mathbf{k}} \hat{\psi}_{\alpha,\mathbf{k}}^\dagger(t) i \partial_t \hat{\psi}_{\alpha,\mathbf{k}}(t) - H(t) \right]. \tag{37}$$

In Eq. (37), the Hamiltonian reads

$$H(t) = \sum_{\alpha,\mathbf{k}} \hat{\psi}_{\alpha,\mathbf{k}}^\dagger(t) \hat{H}_{\alpha,\mathbf{k}} \hat{\psi}_{\alpha,\mathbf{k}}(t) + \sum_{\mathbf{k},\mathbf{q}} (\hat{\psi}_{R,\mathbf{k}}^\dagger(t) \hat{T}(t) \hat{\psi}_{L,\mathbf{q}}(t) + \mathrm{H.c.}),$$

where $\hat{H}_{\alpha,\mathbf{k}}$ is the matrix Hamiltonian of the BCS leads,

$$\hat{H}_{\alpha,\mathbf{k}} = \begin{pmatrix} \xi_{\mathbf{k}} & i\sigma_y \Delta_\alpha \\ -i\sigma_y \Delta_\alpha^* & -\xi_{\mathbf{k}} \end{pmatrix}, \tag{38}$$

and $\hat{T}(t)$ is the matrix tunnel amplitude,

$$\hat{T}(t) = \begin{pmatrix} T(t) & 0 \\ 0 & -T^*(t) \end{pmatrix}, \tag{39}$$

where $T(t) = T_0 + T_\parallel \sigma_z + T_\perp \sigma_x e^{-i\sigma_z \Omega t}$, see Eq. (7). Defining the time-dependent unitary matrix as

$$\hat{\mathcal{U}}(t) = \begin{pmatrix} e^{i\sigma_z \Omega/2t} & 0 \\ 0 & e^{-i\sigma_z \Omega/2t} \end{pmatrix} = e^{i\hat{\sigma}_3 \Omega/2t}, \tag{40}$$

where the 4×4 Pauli spin matrix $\hat{\sigma}_3$ was defined in Eq. (36), the field operators transform as

$$\hat{\bar{\psi}}_{\alpha,\mathbf{k}}^\dagger(t) = \hat{\psi}_{\alpha,\mathbf{k}}^\dagger(t) \hat{\mathcal{U}}(t), \quad \hat{\bar{\psi}}_{\alpha,\mathbf{k}}(t) = \hat{\mathcal{U}}^\dagger(t) \hat{\psi}_{\alpha,\mathbf{k}}(t).$$

It is then straightforward to check that this unitary transformation leaves the BCS Hamiltonian, see Eq. (38), invariant while the transmission matrix, see Eq. (39), becomes time independent,

$$\hat{\bar{T}} = \hat{\mathcal{U}}^\dagger(t) \hat{T}(t) \hat{\mathcal{U}}(t) \equiv \hat{T}(\Omega = 0). \tag{41}$$

The unitary-transformed action therefore corresponds to the one of a static tilted spin with an effective magnetic field, h_z, acting on the leads,[54]

$$S[\hat{\bar{\psi}}, \hat{\bar{\psi}}^\dagger] = \int_{\mathcal{C}} dt \left[\sum_{\alpha, \mathbf{k}} \hat{\bar{\psi}}^\dagger_{\alpha, \mathbf{k}} (i\partial_t - h_z \hat{\sigma}_z) \hat{\bar{\psi}}_{\alpha, \mathbf{k}} - \tilde{H} \right]. \quad (42)$$

In Eq. (42), the transformed Hamiltonian is time independent and equals the Hamiltonian of Eq. (1) with zero precession frequency. The latter has been absorbed in the effective magnetic field,

$$h_z = \frac{\Omega}{2}, \quad (43)$$

acting on the superconducting leads. From Eq. (43), we recover the fact, already noticed in Sec. III, that the precession frequency corresponds to an effective Zeeman splitting energy.

Gauging out the precession frequency in the transmission term is equivalent to the usual transformation of going from the laboratory frame, where the spin is precessing, to the rotating frame where the spin appears to be static, see Fig. 1(b). The transformation is related to the peculiar harmonic dependence of the spin-flip transmission amplitude on time, see Eq. (7), and implies that the problem has a *steady-state* solution. It allows us to replace the time-dependent problem by a time-independent one at the expense of dealing with a static problem with noncolinear magnetization. Indeed, the effective magnetic field in the leads, h_z, is oriented along the z axis whereas the spin in the junction is tilted in an arbitrary direction fixing the amplitudes $T_\parallel$ and $T_\perp$. However, the system is out of equilibrium no matter what frame one considers. In particular, in the rotating frame, the out-of-equilibrium nature of the problem is related to the nontrivial action of the effective magnetic field on the Green's functions of the leads, i.e., with respect to what a usual magnetic field would do. We will show this in the next paragraph and end this one with a simple relation between the Green's functions in both frames.

The Green's functions are matrices in spin ⊗ Nambu space and are defined with the help of

$$\hat{g}_{\alpha, \beta}(t, t') = -i\langle \mathcal{T}_{\mathcal{C}} \hat{\psi}_\alpha(t) \hat{\psi}^\dagger_\beta(t') \rangle, \quad (44)$$

where $\mathcal{T}_{\mathcal{C}}$ is the time-ordering operator, for the Grassmann fields, along the $\mathcal{C}$ contour and $\alpha, \beta = R, L$ are lead indices [see Eq. (48) with $h_z = 0$ for the form of the matrix Green's function]. The unitary transformation then allows the following correspondence between the Green's functions in both frames:

$$\hat{\bar{g}}_{\alpha, \beta}(t, t') = \hat{\mathcal{U}}^\dagger(t) \hat{g}_{\alpha, \beta}(t, t') \hat{\mathcal{U}}(t'). \quad (45)$$

B. Consequences for the leads

Before using the unitary transformation to compute the transport properties of the junction, we start by focusing on its consequences at the level of the leads (Green's functions, gap equation, and thermodynamic quantities).

1. Green's functions

To deal with the steady-state out-of-equilibrium situation we are considering, we will use the standard Keldysh tech-

nique, see, e.g., Ref. 55 for reviews, and compute the Green's functions on a closed time or Keldysh, $\mathcal{C}_K$, contour. This procedure leads to a doubling of the degrees of freedom by introducing ψ_+ fields on the upper, forward, branch and ψ_- fields on the lower, backward, branch. Therefore, besides the usual retarded, $\hat{g}^R$, and advanced, $\hat{g}^A$, Green's functions defined in Sec. III, there will be an additional component,

$$\hat{g}^-_{\alpha, \beta}(t, t') = -i\langle \mathcal{T}_{\mathcal{C}_K} \psi_{+, \alpha}(t) \psi^\dagger_{-, \beta}(t') \rangle, \quad (46)$$

which is the lesser Keldysh function. In what follows, we will work with $\hat{g}^-$, keeping in mind that it is related to the standard Keldysh Green's function, $\hat{g}^K$, with the help of the following identity, $\hat{g}^K = \hat{g}^R - \hat{g}^A + 2\hat{g}^-$.

The unitary transformation of Eq. (45) will therefore not only affect the spectral Green's functions (retarded and advanced) but also the Keldysh Green's function which contains information about the occupation of states and hence the out-of-equilibrium properties of the system. For noninteracting leads, the lesser component reads

$$\hat{g}^{(0)-}_{\alpha, \beta}(t, t') = -\delta_{\alpha, \beta} n^\alpha_F \circ (\hat{g}^{(0)R}_\alpha - \hat{g}^{(0)A}_\alpha)(t, t'), \quad (47)$$

where n^α_F is the Fermi occupation function in lead α, the retarded and advanced functions were defined in Eq. (14) and the symbol ∘ implies time convolution.

In spin ⊗ Nambu space, the result of the unitary transformation on the spectral quasiclassical matrix Green's function reads

$$\hat{\bar{g}}_\alpha(i\omega) = \begin{pmatrix} g_\alpha(i\omega_+) & 0 & 0 & -f_\alpha(i\omega_+) \\ 0 & g_\alpha(i\omega_-) & f_\alpha(i\omega_-) & 0 \\ 0 & f^\dagger_\alpha(i\omega_-) & g_\alpha(i\omega_-) & 0 \\ -f^\dagger_\alpha(i\omega_+) & 0 & 0 & g_\alpha(i\omega_+) \end{pmatrix}, \quad (48)$$

where $i\omega_\pm = i\omega \pm h_z$. At the level of the advanced and retarded Green's functions, Eq. (48) shows that the effective magnetic field acts in a way similar to a usual magnetic field.

The unusual nature of the present magnetic field appears from the effect of the unitary transformation on the Keldysh component of the Green's function,

$$\hat{\bar{g}}^{(0)-}_{\alpha, \beta}(t, t') = -\delta_{\alpha, \beta} \hat{\bar{n}}^\alpha_F \circ (\hat{\bar{g}}^{(0)R}_\alpha - \hat{\bar{g}}^{(0)A}_\alpha)(t, t'), \quad (49)$$

and equivalently for the function $\hat{\bar{g}}^K$. Equation (49) shows that, contrary to what happens with a usual magnetic field, the occupation function is also affected by the transformation. The latter becomes a matrix in spin ⊗ Nambu space and reads

$$\hat{\bar{n}}^\alpha_F(t) = n^\alpha_F(t) \hat{\mathcal{U}}^\dagger(t) = n^\alpha_F(t) e^{-i\hat{\sigma}_z \Omega/2 t}. \quad (50)$$

Though the system is in a steady state, as it has been shown in Sec. IV A, the very fact that the time-dependent unitary transformation modifies the occupation functions reflects the out-of-equilibrium nature of the problem. For example, we recover the fact that the spin accumulation (the difference in chemical potential between spin-up and spin-down particles),

$$\vec{\mu}^s = \int_0^\infty d\epsilon \, \text{Tr}[\hat{\vec{\sigma}} \hat{n}_F(\epsilon)] \tag{51}$$

is nonzero only in the z direction and, at $T=0$, has an amplitude, $\mu_z^s(T=0)=\Omega$, corresponding to the splitting between spin-up and spin-down bands, see Fig. 1(b).

2. Density of states

In the rotated frame, the BCS density of states (DOS) of a given lead subject to the effective magnetic field reads

$$\tilde{\rho}_{\uparrow,\downarrow}(\epsilon) = \nu_N \frac{|\epsilon \mp h_z|}{\sqrt{(\epsilon \mp h_z)^2 - \Delta^2}}. \tag{52}$$

Such a DOS is similar to the one determined by Tedrow and Meservey[1] and has been schematically represented in Fig. 1(b). In particular, an effective (precession-frequency dependent) gap of $2\Delta - 2h_z$ between spin-up and spin-down quasiparticle bands appears. For $\Omega = 2\Delta$, the spin-up and spin-down quasiparticle peaks overlap. This is another manifestation of the fact that the nonanalyticity of the current at $\Omega = 2\Delta$, see Eq. (19), originates from extended states.

3. Gap equation and thermodynamic properties

Another proof of the unusual nature of the effective magnetic field is that it has no effect on the superconducting gap Δ. This can be seen from the gap equation, $\Delta_\alpha = V_0 f_\alpha(\tau=0)$, where V_0 is the effective attractive coupling, which involves the equal-time component of the anomalous part of the quasiclassical BCS Green's function. The gap equation is therefore invariant under the unitary transformation. The effective magnetic field we are considering does not affect superconductivity in the leads in a way similar to a usual magnetic field.

More generally, the thermodynamic properties of the leads involve energy integrations over products of the DOS and the occupation function. Changing variables of integration therefore eliminates the effective magnetic field and makes these quantities invariant under the unitary transformation.

C. Transport equations

With the help of the unitary transformation of Sec. IV A, we derive in this paragraph general transport formulas valid for a junction of arbitrary transparency. To this end, we will follow the standard approach of computing the current from the Keldysh Green's function, see Refs. 56 and 57 for some references on the subject.

In the compact spin $\otimes$ Nambu space, the charge and spin current operators are defined as

$$\hat{I}^c(t) = -ie \sum_{\mathbf{k,q}} \hat{\psi}_{R,\mathbf{k}}^\dagger(t) \hat{\sigma}_0 \hat{T}(t) \hat{\psi}_{L,\mathbf{q}}(t),$$

$$\hat{\mathbf{I}}^s(t) = \frac{i}{2} \sum_{\mathbf{k,q}} \hat{\psi}_{R,\mathbf{k}}^\dagger(t) \hat{\vec{\sigma}}^s \hat{T}(t) \hat{\psi}_{L,\mathbf{q}}(t), \tag{53}$$

where $\hat{\vec{\sigma}}^s = (\hat{\sigma}_1, \hat{\sigma}_2^s, \hat{\sigma}_3)$ give the three components of the spin current, the $\hat{\sigma}_i$ $(i=0,1,2,3)$ were defined in Eq. (36) and $\hat{\sigma}_2^s = \hat{\sigma}_2 \hat{\sigma}_0$. Taking the average of the current yields

$$I^c(t) = e \, \text{Tr}[\hat{\sigma}_0 \hat{T}(t) \hat{g}_{LR}^-(t,t)], \tag{54a}$$

$$\mathbf{I}^s(t) = -\frac{1}{2} \text{Tr}[\hat{\vec{\sigma}}^s \hat{T}(t) \hat{g}_{LR}^-(t,t)], \tag{54b}$$

where $\hat{g}_{LR}^-(t,t')$ is the lesser Keldysh Green's function defined in Eq. (46) and the currents are, *a priori*, time dependent. As in Sec. III, the current is computed at a given electrode and the lead index is dropped for simplicity.

The computation of the current in Eq. (54) therefore reduces to the computation of the Keldysh Green's function. Treating the transmission amplitude $\hat{T}$ as the perturbation the latter satisfies the following Dyson equation:

$$\check{g}^-(t,t') = [1 + \check{g}^R \circ \check{T}] \circ \check{g}^{(0)-} \circ [1 + \check{T} \circ \check{g}^A](t,t'), \tag{55}$$

where the free lesser Keldysh Green's function was given in Eq. (47). In Eq. (55), the check denotes the fact that all matrices are 8×8 matrices in the left-right $\otimes$ spin $\otimes$ Nambu space,

$$\check{g} = \begin{pmatrix} \hat{g}_{RR} & \hat{g}_{RL} \\ \hat{g}_{LR} & \hat{g}_{LL} \end{pmatrix}, \quad \check{T} = \begin{pmatrix} 0 & \hat{T} \\ \hat{T} & 0 \end{pmatrix} \tag{56}$$

and symmetric contacts have been assumed. The dressed retarded and advanced Green's functions, $\check{g}^{R,A}$, also satisfy their own Dyson equation,

$$\check{g}^{R(A)}(t,t') = \check{g}^{(0)R(A)}(t,t') + \check{g}^{(0)R(A)} \circ \check{T} \circ \check{g}^{R(A)}(t,t'), \tag{57}$$

where $\hat{g}^{(0)R(A)}$ are given by the proper analytic continuation of Eq. (14).

In the dc limit, that we are interested in, Eq. (55) may be further simplified by assuming that both electrodes have identical occupation functions, $n_F^\alpha \equiv n_F$ does not depend on $\alpha = L,R$, as no bias is applied. This yields

$$\check{g}^-(t,t') = -(\check{g}^R \circ n_F - n_F \circ \check{g}^A)(t,t')$$
$$- \check{g}^R \circ (n_F \circ \check{T} - \check{T} \circ n_F) \circ \check{g}^A(t,t'), \tag{58}$$

which shows that the computation of the Keldysh Green's function further reduces to the computation of the retarded and advanced functions. Notice that, because $\hat{T}(t)$ is locally time dependent, the second term in Eq. (58) is nonzero for the present problem.

The coupled Eqs. (57) and (58) are integral equations which are quite complicated to solve, in general. Remarkably, the present problem considerably simplifies by going to the rotated frame. With the help of the unitary transformation of Sec. IV A, the Dyson equation for the lesser Keldysh function becomes

$$\check{\tilde{g}}^-(t,t') = -(\check{\tilde{g}}^R \circ \check{\tilde{n}}_F - \check{\tilde{n}}_F \circ \check{\tilde{g}}^A)(t,t')$$
$$- \check{\tilde{g}}^R \circ (\check{\tilde{n}}_F \check{\tilde{T}} - \check{\tilde{T}} \check{\tilde{n}}_F) \circ \check{\tilde{g}}^A(t,t'), \tag{59}$$

where $\check{\tilde{T}}$ is time independent (and real) which eliminates a time convolution. The noncommutativity between the transmission amplitude matrix and the occupation function is preserved because the latter becomes a matrix, $\check{\tilde{n}}_F$, in the rotated

frame. Similarly, the Dyson equations for the retarded and advanced functions, Eq. (57), become

$$\check{\bar{g}}^{R(A)}(t,t') = \check{\bar{g}}^{(0)R(A)}(t,t') + \check{\bar{g}}^{(0)R(A)}\check{T} \circ \check{\bar{g}}^{R(A)}(t,t'), \quad (60)$$

and another time convolution has been eliminated. This implies that all Green's functions in the rotated frame depend on the difference of their time arguments which allows us to go to Fourier space. Extracting the left-right component of Eq. (59) yields

$$\hat{\bar{g}}_{LR}^{<}(\omega) = -[\hat{\bar{g}}_{LR}^{R}(\omega)\hat{\bar{n}}_F(\omega) - \hat{\bar{n}}_F(\omega)\hat{\bar{g}}_{LR}^{A}(\omega)]$$
$$- \hat{\bar{g}}_{LR}^{R}(\omega)[\hat{\bar{n}}_F(\omega)\hat{\bar{T}} - \hat{\bar{T}}\hat{\bar{n}}_F(\omega)]\hat{\bar{g}}_{LR}^{A}(\omega)$$
$$- \hat{\bar{g}}_{LL}^{R}(\omega)[\hat{\bar{n}}_F(\omega)\hat{\bar{T}} - \hat{\bar{T}}\hat{\bar{n}}_F(\omega)]\hat{\bar{g}}_{RR}^{A}(\omega), \quad (61)$$

where $\hat{\bar{n}}_F$ is given by Eq. (50) and $\hat{\bar{T}}$ by Eqs. (39) and (41). Notice that the last two terms in Eq. (61) are nonzero only because the system is out of equilibrium, i.e., the precession frequency is nonzero. Formally, they appear as collision terms where the occupation function is brought away from its equilibrium value.

Similarly, the Dyson equations for the retarded and advanced functions, Eq. (57), reduce to a set of algebraic equations which are straightforward to solve, yielding

$$\hat{\bar{g}}_{LR}^{R(A)}(\omega) = D_{L,R}^{(0)R(A)-1}\hat{\bar{g}}_{L}^{(0)R(A)}(\omega)\hat{\bar{T}}\hat{\bar{g}}_{R}^{(0)R(A)}(\omega),$$

$$\hat{\bar{g}}_{RR}^{R(A)}(\omega) = D_{L,R}^{(0)R(A)-1}\hat{\bar{g}}_{R}^{(0)R(A)}(\omega),$$

$$\hat{\bar{g}}_{LL}^{R(A)}(\omega) = D_{L,R}^{(0)R(A)-1}\hat{\bar{g}}_{L}^{(0)R(A)}(\omega), \quad (62)$$

where the denominator reads

$$D_{\alpha,\beta}^{(0)R(A)} = \mathbf{1}_4 - \hat{\bar{g}}_{\alpha}^{(0)R(A)}(\omega)\hat{\bar{T}}\hat{\bar{g}}_{\beta}^{(0)R(A)}(\omega)\hat{\bar{T}}, \quad (63)$$

the indices $\alpha, \beta = R, L$ and $\mathbf{1}_4$ is the unit matrix in four-dimensional space. In Eqs. (62) and (63), the noninteracting Green's functions depend on the effective magnetic field, see Eq. (48).

Substituting the expressions of Eq. (62) in Eq. (61) yields the lesser Keldysh Green's function. The latter has then to be substituted in the expression of the current in order to compute the transport properties of the junction. To this end, we have to express the current, Eq. (54), in terms of the transformed Green's functions,

$$I^c = e \int \frac{d\omega}{2\pi} \text{Tr}[\hat{\sigma}_0 \hat{\bar{T}} \hat{\bar{g}}_{LR}^{<}(\omega)], \quad (64a)$$

$$\mathbf{I}^s(t) = -\frac{1}{2} \int \frac{d\omega}{2\pi} \text{Tr}[\hat{\bar{\sigma}}^s(t) \hat{\bar{T}} \hat{\bar{g}}_{LR}^{<}(\omega)]. \quad (64b)$$

Equation (64a) shows that the charge current is actually time independent. On the other hand, Eq. (64b), shows that the spin current is circularly polarized in the xy plane whereas the z component is time independent. This comes from the fact that $\hat{\bar{\sigma}}^s(t) = [\hat{\bar{\sigma}}_1(t), \hat{\bar{\sigma}}_2^s(t), \hat{\sigma}_3]$, where

$$\hat{\bar{\sigma}}_1(t) = \hat{\sigma}_1 e^{-i\hat{\sigma}_3 \Omega t}, \quad \hat{\bar{\sigma}}_2^s(t) = \hat{\sigma}_2^s e^{-i\hat{\sigma}_3 \Omega t}. \quad (65)$$

These results agree with the results of Sec. III.

Formally, Eq. (64) together with Eqs. (61) and (62) as well as the self-consistent gap equation, allow for an exact computation of the charge and spin currents at any temperature, value of the precession frequency and transparency of the junction. Practically, the analytical computation of the current in the transparent limit is extremely tedious in the general case. As it will be shown in Sec. V, analytic calculations can easily be performed for a nontilted/static spin and may be significantly simplified in the case where the spin has a large tilt angle $\theta \to \pi/2$, see also Refs. 37 and 38. In the general case, however, these equations have to be solved numerically. It turns out that, within the present reformulation and simplification of the problem, the numerical implementation is quite straightforward. Indeed, the system of equations above has the same form as the one for an equilibrium problem. Out-of-equilibrium effects simply appear as effective magnetic field dependencies of the noninteracting Green's functions, the matrix occupation function as well as the sigma matrices of the spin current.

V. RESULTS FOR THE CHARGE CURRENT

The main quantity of interest in this section is the charge current which has been computed in the tunnel limit in Sec. III and for which a formal exact expression in the transparent was given in Sec. IV C, see Eq. (64a) together with Eqs. (61) and (62). We will start from the simplest cases (zero precession frequency, large tilt angle) before going to the general case where a fully numerical approach is required. Besides the current itself, we will also be interested in the current-carrying states, the nature of which will help us interpret the results obtained for the current. Information on these current-carrying states, as well as their occupation, is contained in the (charge) current kernel,

$$I^c(\omega) = e \, \text{Tr}[\hat{\sigma}_0 \hat{\bar{T}} \hat{\bar{g}}_{LR}^{<}(\omega)], \quad I^c = \int \frac{d\omega}{2\pi} I^c(\omega). \quad (66)$$

By definition, the poles of the current kernel, or zeros of Eq. (63) (when they do exist), correspond to well-defined bound states with energies below the superconducting gap. The current due to these Andreev states may formally be written as

$$I_{ABS}^c = \int_{-\Delta(h_z)}^{+\Delta(hz)} \frac{d\omega}{2\pi} I^c(\omega), \quad (67)$$

where the limits of integration may be affected by the precession of the spin. On the other hand, the branch cut structure of the current kernel implies that extended states may carry the current as well, see Sec. III where this fact has already been discussed in the tunnel limit. The current due to these extended may be formally written as

$$I_{ext}^c = \int_{-\infty}^{-\Delta(hz)} \frac{d\omega}{2\pi} I^c(\omega) + \int_{+\Delta(h_z)}^{+\infty} \frac{d\omega}{2\pi} I^c(\omega), \quad (68)$$

such that the total current $I^c = I_{ABS}^c + I_{ext}^c$. In general, localized and extended states compete in order to carry the current.[58]
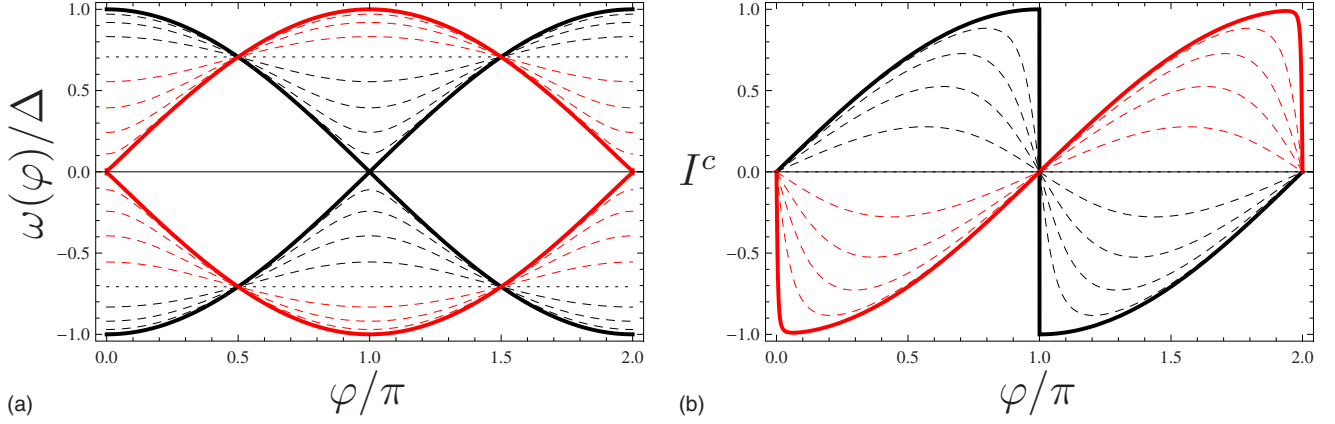
FIG. 4. (Color online) (a) The spectrum of Andreev bound states and (b) the charge current for a static spin with $t_0 = 1 - t_S$ and t_S varies from 0 (thick solid black line) to 1 (thick solid red line) with a step of 0.1.

This will clearly be seen at the level of the current and its dependence on the precession frequency and/or superconducting phase difference. The goal of this section is to discuss these facts.

In the following, numerical simulations are performed with a small energy relaxation rate that takes into account phenomenologically the damping of the quasiparticles due to inelastic processes, such as, e.g., electron-phonon interactions, in the leads. We will use $\eta = 10^{-3}\Delta$, which agrees with typical estimates[60] for usual superconductors, where Δ corresponds to the $T=0$ amplitude of the superconducting order parameter. Moreover, we will run the simulations at low temperatures, $T = 10^{-3}\Delta$, unless specified.

A. Static spin in the junction ($\Omega = 0$)

In the case where the spin in the junction is static, only the first term in the expression of the Keldysh Green's function, Eq. (61), gives a nonzero contribution to the current. Some matrix algebra yields a simple analytic expression for the current kernel,

$$I^c(w) = 2e(\mathcal{T}_0 - \mathcal{T}_S)\Delta^2 \sin\varphi \, n_F[\omega]\mathrm{Im}\left\{\frac{1}{(\omega + i\eta)^2 - \omega^2(\varphi)}\right\}, \quad (69)$$

where $\eta = 0^+$, the transparencies of the junctions are defined as

$$\mathcal{T}_0 = \frac{4t_0^2}{(1 + t_0^2 - t_S^2)^2 + 4t_S^2}, \quad \mathcal{T}_S = \frac{4t_S^2}{(1 + t_0^2 - t_S^2)^2 + 4t_S^2}, \quad (70)$$

and, due to the spin-rotational invariance of the static problem, t_S combines both spin-conserving as well as spin-flip tunneling amplitudes, $t_S^2 = t_\parallel^2 + t_\perp^2$. From Eq. (69), we see that the current kernel has two poles at $\omega_\pm(\varphi) = \pm\omega(\varphi)$, where

$$\omega(\varphi) = \Delta\sqrt{1 - \mathcal{T}_0\sin^2(\varphi/2) - \mathcal{T}_S\cos^2(\varphi/2)}. \quad (71)$$

These poles correspond to bound states with energies below the superconducting gap, $\omega(\varphi) \leq \Delta$, see Fig. 4(a). The integration of the current kernel reduces to an integration over these poles which therefore carry all the charge current

across the junction. As can be seen from Eq. (69), the Andreev bound states carry current in opposite directions,

$$I^c_\pm = \mp 2e\frac{d\omega(\varphi)}{d\varphi}n_F[\pm\omega(\varphi)], \quad (72)$$

where because of the absence of any current-carrying extended state, the total current is given by $I^c = I^c_+ + I^c_-$. The Fermi function then guarantees that, at low-enough temperatures, only the lowest subgap state is occupied yielding a nonzero supercurrent,

$$I^c = \frac{e(\mathcal{T}_0 - \mathcal{T}_S)\Delta \sin\varphi}{2\sqrt{1 - \mathcal{T}_0\sin^2(\varphi/2) - \mathcal{T}_S\cos^2(\varphi/2)}}\tanh\left[\frac{\omega(\varphi)}{2T}\right], \quad (73)$$

which is plotted in Fig. 4(b).

With these formulas in hand, we now consider the well-known case[59] where $t_S = 0$ and t_0 is arbitrary. In this case, the spectrum of the Andreev bound state reads $\omega(\varphi) = \Delta\sqrt{1 - \mathcal{T}_0\sin^2(\varphi/2)}$ with $\mathcal{T}_0 = 4t_0^2/(1 + t_0^2)^2$. Assuming that we are at zero temperature, only the lowest in energy of these Andreev states is occupied. We see from the thick black curve in Fig. 4(a) that it has a minimum in energy at $\varphi = 0$, which therefore corresponds to its ground-state phase difference. The current of such a 0 junction may be straightforwardly obtained from Eq. (73) and it is plotted on the thick black curve of Fig. 4(b). On the other hand, for $t_0 = 0$ and t_S arbitrary, the spectrum of the Andreev bound state, $\omega(\varphi) = \Delta\sqrt{1 - \mathcal{T}_S\cos^2(\varphi/2)}$ with $\mathcal{T}_S = 4t_S^2/(1 + t_S^2)^2$, has a ground-state phase difference of $\varphi = \pi$, see the thick red curve in Fig. 4(a). The current of such a π junction is the opposite of the one of a 0 junction, see Eq. (73) and the thick red curve of Fig. 4(b). As was anticipated in Sec. III A, when $t_0 = t_S$, a transition from a 0 to a π junction takes place. This is shown in Fig. 4 where it can be seen that, as soon as t_S is nonzero, the bound-state spectrum disconnects from the continuum at $\pm\Delta$. Increasing t_S, the curvature of the Andreev levels changes sign once $t_S > t_0$ which corresponds to exchanging the minimum and maximum bound-state energies and is equivalent to a π shift of the phase.

B. Precessing spin in the junction ($\theta \approx \pi/2$)

When the spin in the junction is precessing, significant deviations from the results of Sec. V A are obtained. In this section, we consider the limit where the tilt angle of the spin with respect to the precession axis is large, $\theta \approx \pi/2$. From Eq. (8) this implies that $t_\parallel \approx 0$. For simplicity, we further assume that $t_0 = 0$. Tunneling is then only possible via spin-flip processes through an in-plane precessing spin. This case

$$\omega(\varphi) = \sqrt{h_z^2 + \frac{\Delta^2}{1 - \widetilde{\mathcal{T}}} \left\{ 1 + \widetilde{\mathcal{T}} \cos\varphi - \sqrt{\widetilde{\mathcal{T}^2}(1 + \cos\varphi)^2 + 4(1 - \widetilde{\mathcal{T}})\left(\frac{h_z}{\Delta}\right)^2} \right\}}, \qquad (74)$$

where the transparency of the junction was redefined as $\widetilde{\mathcal{T}} = 2t_\perp^2/(1 + t_\perp^4)$. Equation (74) considerably differs from the corresponding expression in the equilibrium case, Eq. (71). Indeed, Eq. (74) shows that the Andreev spectrum depends now on the precession frequency via h_z. Moreover, the appearance of the square roots suggests that bound states and extended states are interrelated. This is more easily seen from the asymptotic expressions of the bound-state spectrum,

$$\omega(\varphi) = \begin{cases} \Delta|1 - \widetilde{h}_z|, & \widetilde{\mathcal{T}} \to 0 \\ \Delta|\tan(\varphi/2)|\sqrt{\cos^2(\varphi/2) - \widetilde{h}_z^2}, & \widetilde{\mathcal{T}} \to 1, \end{cases} \qquad (75)$$

where $\widetilde{h}_z = h_z/\Delta$ is the reduced effective magnetic field. Equation (75) shows that, in the tunnel regime where $\widetilde{\mathcal{T}} \to 0$, the Andreev bound states are dispersionless and cross at $h_z = \Delta$. This can be contrasted with the equilibrium behavior ($h_z = 0$) where they touch the continuum of states [this can also be seen from Eq. (71) with $\mathcal{T}_0, \mathcal{T}_1 \to 0$]. In both cases, however, extended states carry all the current (in the out-of-equilibrium case, the currents of both Andreev bound states cancel each other). This agrees with the results of Sec. III A. On the other hand, in the transparent limit where $\widetilde{\mathcal{T}} \to 1$, the Andreev spectrum depends on the superconducting phase. As can be seen from Eq. (75), the bound states merge with the continuum of states for high enough values of h_z and/or a phase difference close to π. As has been shown in Refs. 37 and 38, this merging takes place at a phase difference φ_c such that $d\omega(\varphi_c)/d\varphi = 0$. In the transparent limit, this leads to the following relation between the critical phase and effective magnetic field: $h_{z,c}(\varphi) = \Delta \cos^2(\varphi/2)$ or equivalently $\varphi_c(h_z) = 2 \arccos(\sqrt{h_z/\Delta})$. Hence, bound states exist for phase differences smaller than φ_c and larger than $2\pi - \varphi_c$. For other phase differences, the extended states carry all the current. Notice that, from these arguments, the average critical field at which bound states and extended states merge in the transparent limit is given by

has been reported on in Refs. 37 and 38. We will summarize below the basic results related to the nature of the current-carrying states and compare them with the results of Sec. V A.

In the case of a spin precessing in the plane, the simplest quantity which may be extracted analytically is the spectrum of the bound states. The latter correspond to the poles of the current kernel of Eq. (66) [or equivalently to the zeros of Eq. (63)]. Some algebra yields

$$\bar{h}_{z,c} = \int_0^{2\pi} \frac{d\varphi}{2\pi} h_{z,c}(\varphi) = \frac{\Delta}{2}. \qquad (76)$$

In order to illustrate these facts on a concrete example, the density of states in the rotated frame has been plotted in Fig. 5(a), for the special case where $\widetilde{\mathcal{T}} = 1$ and $h_z = 0.25\Delta$. From the previous arguments, the critical phase associated with this value of the effective magnetic field is given by $\varphi_c \approx 0.67\pi$. This is confirmed by Fig. 5(a) which shows that subgap states exist for $\varphi < \varphi_c$ and that they tend to merge with the continuum of states, located at $\pm(\Delta - h_z)$, as φ approaches φ_c. For $\varphi > \varphi_c$ (not represented on the figure), there are no more bound states. The corresponding low-T current kernel has been plotted in Fig. 5(b). In accordance with this figure, the total charge current may be decomposed in the following way ($h_z < \Delta$):

$$I^c = \left\{ \int_{-\Delta+h_z}^{\Delta-h_z} + \int_{-\Delta-h_z}^{-\Delta+h_z} + \int_{\Delta-h_z}^{\Delta+h_z} \right\} \frac{d\omega}{2\pi} I^c(\omega), \qquad (77)$$

where the first integral is over poles, $\omega(\varphi)$, corresponding to current-carrying bound states whereas the last two integrals are over branch cuts, of width $2h_z$ around $\pm\Delta$, corresponding to current-carrying extended states. The integral has to be computed numerically which will be done in the next paragraph. However, we already see from Fig. 5(b) that, for $\varphi \approx 0$ (black curve), both Andreev levels are occupied while for intermediate values of the phase, $\varphi \approx 0.25\pi$ (blue curve), only a single Andreev state is occupied and that at larger values of the phase extended states become the main current-carrying states. These sharp changes in the occupancy of the Andreev states as a function of the phase difference will be seen as a strong suppression of the current in the current-phase relation (CPR) around $\varphi \approx 0$ in the next paragraph.

C. Precessing spin in the junction (arbitrary θ)

For arbitrary tilt angles Eq. (64a) of Sec. IV C does not reduce to any simple analytic form and we proceed numeri-
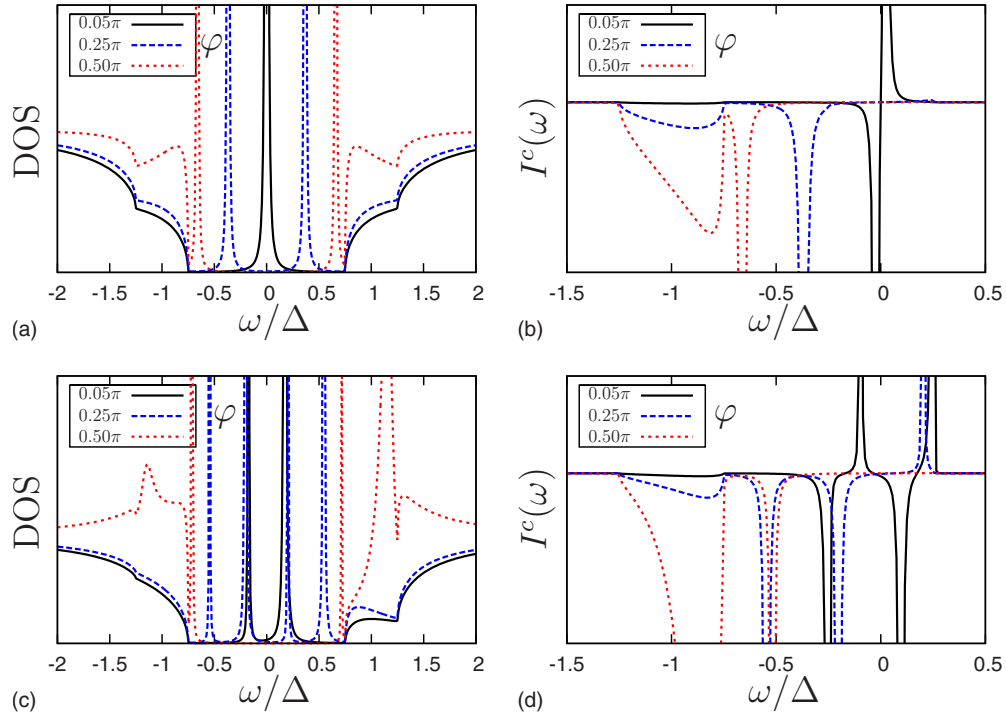
FIG. 5. (Color online) Density of states (DOS) of spin-up particles in the rotated frame and CCK for $t_0=0$, $t_S=1$, and $h_z=0.25\Delta$. The different line styles (and colors) refer to different values of the superconducting phase difference, φ, see the insets. The four panels correspond to $\theta=\pi/2$ for (a) and (b) and $\theta=\pi/4$ for (c) and (d).

cally. The results for the CPR are displayed in Figs. 6 and 7 in the limit of a π junction ($t_S > t_0 = 0$). We see from these figures that the CPR is characterized by sharp steps leading to a strong suppression of the current around $\varphi \approx 0$ and $\varphi \approx 2\pi$. From Figs. 6 and 7, we see that the steps appear clearly for high transparencies, low-precession frequencies ($\Omega \ll 2\Delta$) and preferably for tilt angles $\theta \approx \pi/4$ or larger. For small tilt angles ($\theta \to 0$), one needs to go to higher Ω in order to single out the steps, see Fig. 6(a). Such a structure of the

CPR originates from the existence of current-carrying bound states which disappear, in favor of current-carrying extended states, at both higher values of the effective magnetic field and intermediate values of the phase difference (in particular, around $\varphi \approx \pi$). The strong suppression of the current is due to an abrupt change in the occupation of the lower and upper Andreev levels, the currents of which cancel each other when they are both occupied.

In the case where $\theta \approx \pi/2$, this agrees with the results of the last paragraph and Figs. 5(a) and 5(b) [see discussion
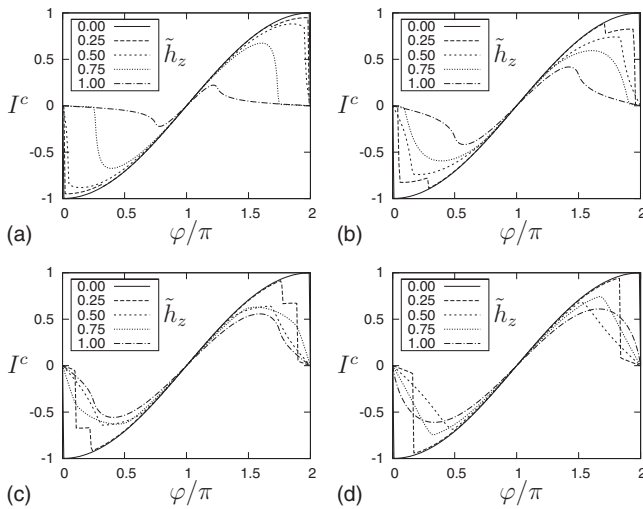

FIG. 6. Charge CPR for fixed transparencies $t_0=0$, $t_S=1$, and different reduced effective magnetic fields, $\tilde{h}_z = h_z/\Delta$, see the insets. The four panels correspond to (a) $\theta=\pi/8$, (b) $\theta=\pi/4$, (c) $\theta=3\pi/8$, and (d) $\theta=\pi/2$. The current is in units of $e\Delta/\hbar$.
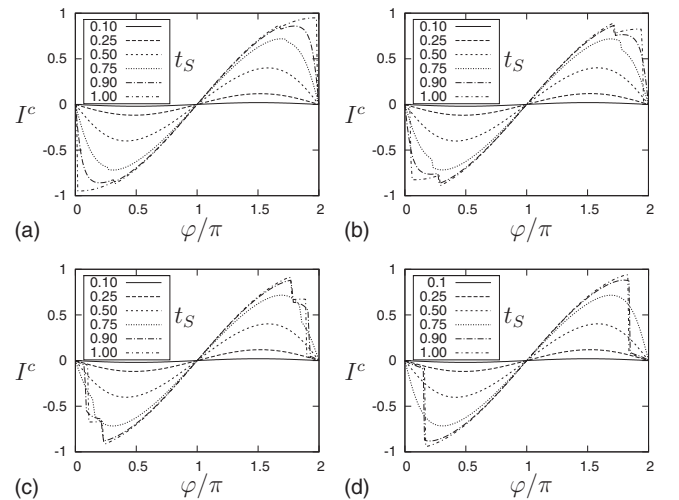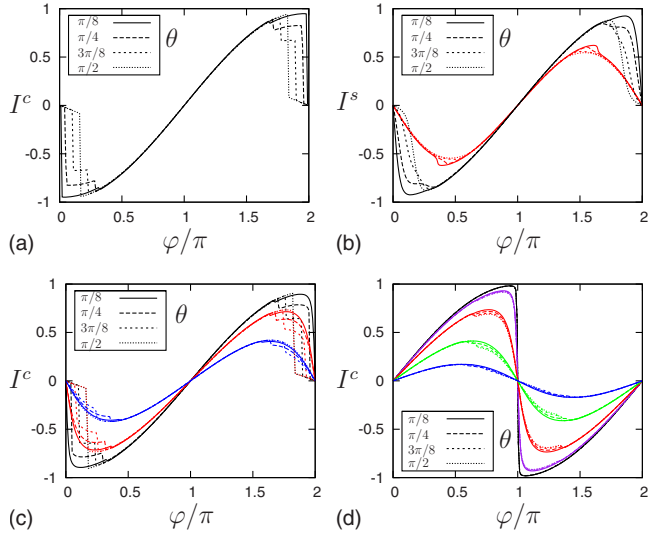

FIG. 7. Charge CPR for a given $h_z=0.25\Delta$ and $t_0=0$. The different line styles refer to different transparencies, t_S, see the insets. The four panels correspond to (a) $\theta=\pi/8$, (b) $\theta=\pi/4$, (c) $\theta=3\pi/8$, and (d) $\theta=\pi/2$. The current is in units of $e\Delta/\hbar$.

FIG. 8. (Color online) Charge CPR for $h_z = 0.25\Delta$. The different line styles refer to different tilt angles, see the insets. The four panels correspond to (a) $t_S = 1$, $t_0 = 0$, and $T = 10^{-3}\Delta$; (b) $t_S = 1$, $t_0 = 0$, and $T = 10^{-2}\Delta$ (black) or $T = 10^{-1}\Delta$ (red); (c) $t_S = 1$, $T = 10^{-3}\Delta$, and $t_0 = 0.25$ (black) or $t_0 = 0.5$ (red) or $t_0 = 0.75$ (blue); (d) $t_0 = 1$, $T = 10^{-3}\Delta$, and $t_S = 0.10$ (black) or $t_S = 0.25$ (purple) or $t_S = 0.5$ (red) or $t_S = 0.75$ (green) $t_S = 0.9$ (blue). The current is in units of $e\Delta/\hbar$.

below Eq. (74)]. This case, which allowed for some analytic estimates, is however rather unphysical. In the more realistic case where $\theta < \pi/2$, we see from Fig. 8(a) that the number of current steps doubles with respect to the case where $\theta = \pi/2$. In the rotating frame, this feature is due to the Zeeman splitting of the Andreev states by the effective magnetic field, which is possible only for intermediate tilt angles. This was shown in Fig. 5(c) for the special case $\theta = \pi/4$. A doubling of the number of bound states can be seen on this figure with respect to Fig. 5(a) for $\theta = \pi/2$. The corresponding current kernel is plotted in Fig. 5(d). The latter shows that for $\varphi \approx 0$ (black curve), all bound states are occupied. Because they carry current in opposite direction, the total current is zero. Upon increasing φ, one bound state is emptied. This leads to a first sharp increase, in absolute value, of the current, e.g., $\varphi \approx 0.25\pi$ (blue curve) in Fig. 5(d). Increasing the value of the phase, another bound state is emptied which leads to a second step in the CPR. Upon further increasing φ, bound states merge with the continuum and the current is again reduced. This doubling of the bound state is special to the rotating frame but allows a convenient interpretation of the results for the current (which does not depend on the frame one considers).

Notice that all these effects are washed out by temperature, see Fig. 8(b) where the parameters have the same values as for Fig. 8(a) except for a raise in temperature. Indeed, by exciting particles from the lower to the upper bound state, temperature broadens the levels and the sharp effects seen at very low temperatures disappear. The effects are also reduced in magnitude when direct tunneling is increased and the π- to 0-junction transition is approached. This is seen from Fig. 8(c) which is valid for a π junction ($t_S = 1 > t_0$) but where t_0 increases from 0.25 (black curves) to 0.75 (blue curves). In the limit of a 0 junction ($t_S < t_0 = 1$), still with a
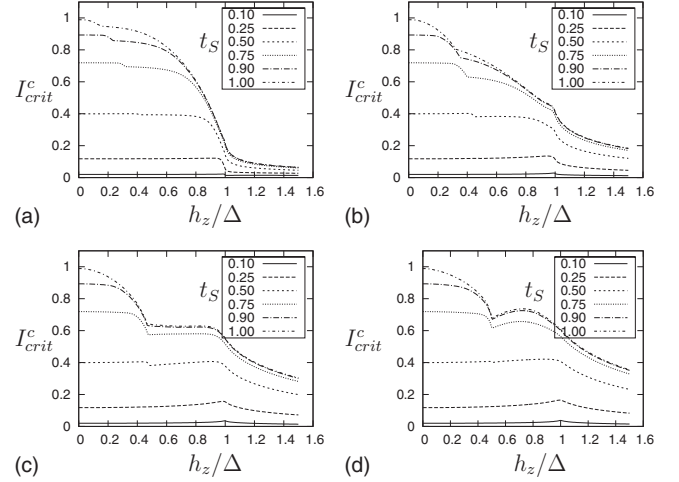

FIG. 9. Absolute value of the charge critical current, i.e., maximum charge current as a function of the phase difference for a given value of h_z. The different line styles refer to different transparencies, t_S, see the insets ($t_0 = 0$). The four panels correspond to (a) $\theta = \pi/8$, (b) $\theta = \pi/4$, (c) $\theta = 3\pi/8$, and (d) $\theta = \pi/2$. The current is in units of $e\Delta/\hbar$.

nonzero tunnel amplitude through the SMM, Fig. 8(d) shows that steps now appear around $\varphi \approx \pi$ but their magnitude is considerably reduced with respect to the case of a π junction. From the point of view of CPR, the low-T π junction is the most interesting, as expected.

In Fig. 9, the critical current, i.e., the maximum current as a function of the phase difference for a given value of h_z, is plotted as a function of h_z. In the tunnel limit, the logarithmic singularity of Eq. (19) is seen at $h_z = 1$. When the transparency of the junction increases, this singularity is broadened and shifted to lower frequencies. This is quite clear from, e.g., Fig. 9(d) (limit where $\theta \to \pi/2$ and $t_S \to 1$) where, upon increasing the transparency, the 2Δ resonance shifts to a kink at the value of the average critical field of Eq. (76) in accordance with the discussion of the last paragraph. When the tilt angle is reduced, the corresponding kink shifts to lower values of the precession frequency, see Figs. 9(a)–9(c).

VI. RESULTS FOR THE SPIN CURRENT

The main quantity of interest in this section is the spin current which was computed in the tunnel limit in Sec. III and for which a formal exact expression in the transparent limit was given in Sec. IV C. Equation (64b) together with Eqs. (61) and (62) as well as the self-consistent gap equation. As was shown in Sec. III, and contrary to the case of the charge current, the spin current can be emitted in the leads only when the spin is precessing so it is a purely out-of-equilibrium effect. It is circularly polarized in the xy plane at the precession frequency, Ω. Moreover, as the results of Sec. III suggest, the spin current is generally emitted for an inclined spin. A computation at an arbitrary tilt angle is therefore required. Nevertheless, the discussion on current-carrying states does not have to be repeated because the spin-current kernel, $\mathbf{I}^s(t,\omega) = e\,\mathrm{Tr}[\hat{\vec{\sigma}}^s(t)\hat{\tilde{T}}\hat{g}_{LR}(\omega)]$, has similar poles
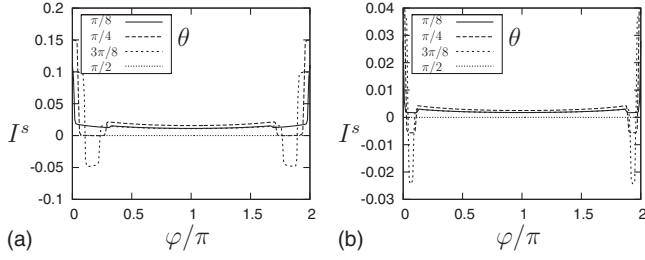
FIG. 10. Spin CPR as a function of the superconducting phase for fixed for $t_S=1$ and $t_0=0$. The different line styles correspond to different tilt angles, see the insets. (a) $h_z=0.25\Delta$ and (b) $h_z=0.1\Delta$. The spin current is in units of $\Delta\hbar/2$.

and branch cuts as the charge current kernel (CCK) of Eq. (66). The spin current will therefore be carried by extended states as well as by bound states, $\mathbf{I}^s=\mathbf{I}^s_{ABS}+\mathbf{I}^s_{ext}$, which are the same as the ones carrying the charge current. This is confirmed by Fig. 10 where it is seen that the amplitude of the spin CPR also has steps as a function of the superconducting phase difference with strong suppression of the spin current around $\varphi\approx0$ in the case of a π junction. For identical values of the parameters, the locations of these steps are the same as for the charge current. Similarly to the case of the charge current, sharp suppressions of the spin current therefore originate from an abrupt change in the occupation of the Andreev levels.

The importance of the spin current is related to its backaction on the motion of the precessing spin in the junction. For simplicity, we will fix the superconducting phase difference to $\varphi=0$ or $\varphi=\pi$, which correspond to the ground-state phase difference of a 0 junction (where $t_S<t_0$) or a π junction (where $t_S>t_0$), respectively. The fact that the spin current may be carried by either extended or bound states allows us then to distinguish between two different sources for the backaction: one from a normal fluid of quasiparticles (the extended states) and the other one from the condensate (the Andreev bound states). Accordingly, the spin-transfer torque will be separated into two contributions,

$$\vec{\tau}^s = \vec{\tau}^s_{ext} + \vec{\tau}^s_{ABS},$$

$$\vec{\tau}^s_{ext} = 2\mathbf{I}^s_{ext} = \frac{\alpha_S(t_S,t_0,T)}{S^2}\mathbf{S}\times\partial_t\mathbf{S}, \qquad (78a)$$

$$\vec{\tau}^s_{ABS} = 2\mathbf{I}^s_{ABS} = \frac{\zeta_S(t_S,t_0,T,\varphi)}{S}\gamma\mathbf{S}\times\mathbf{H}_{eff}, \qquad (78b)$$

where the last equation holds for $\varphi=0$ or $\varphi=\pi$. Equations (78a) and (78b) generalize Eqs. (29) and (26) of the $T=0$ tunnel limit, respectively. In the tunnel limit, the dimensionless coefficients $\alpha_S(t_S,t_0,T)$ and $\zeta_S(t_S,t_0,T,\varphi)$ reduce to the expressions found in Eqs. (32) and (34), respectively. In the general case, they depend on both the transparency of the junction as well as the temperature. Notice that ζ_S also depends on the tilt angle θ, see the cosine term in Eq. (34). In the following, we will fix $\theta=\pi/4$, for simplicity. As already mentioned in Sec. III B, α_S is the Gilbert damping constant
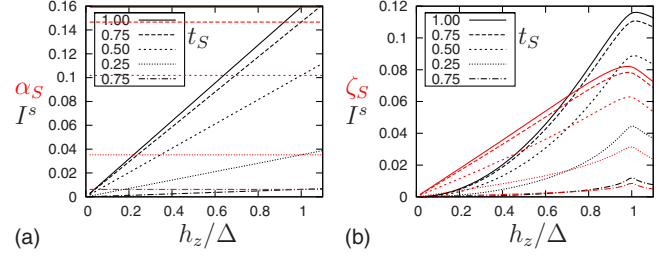

FIG. 11. (Color online) (a) Case of normal leads (limit $\Delta\to0$): absolute value of the quasiparticle spin current (black) and the dimensionless Gilbert damping constant (red) as a function of $\widetilde{h}_z=h_z/\Delta$. (b) Case of superconducting leads: absolute value of the superconducting spin current (black) and the dimensionless shift of the precession frequency (red) as a function of $\widetilde{h}_z=h_z/\Delta$. The different line styles refer to different transparencies, t_S, see the insets. All figures are plotted for fixed: $t_0=0$, $\theta=\pi/4$, $\phi=\pi$, and $T=10^{-3}\Delta$. The spin current is in units of $\Delta\hbar/2$.

due to the normal fluid whereas ζ_S is the precession-frequency shift due to the condensate.

For normal metallic leads, the spin current and the associated Gilbert constant are plotted at very low T as a function of the effective magnetic field in Fig. 11(a) for different transparencies ranging from the tunnel to the transparent limit. This figure shows that the spin current varies linearly as a function of the precession frequency in accordance with the results of the tunnel limit. This pumping of spins from the leads yields a Gilbert constant which depends on the transparency of the junction. This normal contribution does not depend on the phase difference and is only weakly affected by direct tunneling, e.g., $t_0\neq0$. When the leads are superconducting, this low-temperature (T) normal contribution vanishes altogether. The remaining low-T superconducting spin current is plotted in Fig. 11(b) for a π junction ($\varphi=\pi$ and $t_0=0$) as a function of the effective magnetic field and for different values of t_S. In the adiabatic regime ($h_z\ll\Delta$), and actually up to $h_z\approx\Delta$, the superconducting spin current varies quadratically with h_z. In accordance with the tunnel limit results, the corresponding ζ_S is then seen to vary linearly with h_z. From the dependence of the spin current on the precession frequency, we therefore recover the single-particle (linear in h_z) versus two-particle (quadratic in h_z) nature of the normal versus anomalous currents, respectively.

Still in the case of a π junction, the Gilbert and precession-shift constants are plotted in Fig. 12 as a function of temperature, for different values of the transparency t_S and two values of the effective magnetic field: $h_z=0.25\Delta$ [Figs. 12(a) and 12(b)] and $h_z=0.1\Delta$ [Figs. 12(c) and 12(d)]. We see clearly from these two figures that the Gilbert damping is strongly suppressed below temperatures of the order $T\approx0.1T_c$ for $h_z=0.25\Delta$ and $T\approx0.075T_c$ for $h_z=0.1\Delta$, where T_c is the superconducting critical temperature. As shown by Figs. 12(b) and 12(d), which zoom on the low-T region of Figs. 12(a) and 12(c), respectively, the reduction in the damping upon decreasing the temperature goes along with an increasing shift of the precession frequency due to the superconducting spin current. This shift even becomes the dominant effect at low-enough temperatures: $T<0.1T_c$ for $h_z=0.25\Delta$ and $T<0.075T_c$ for $h_z=0.1\Delta$.
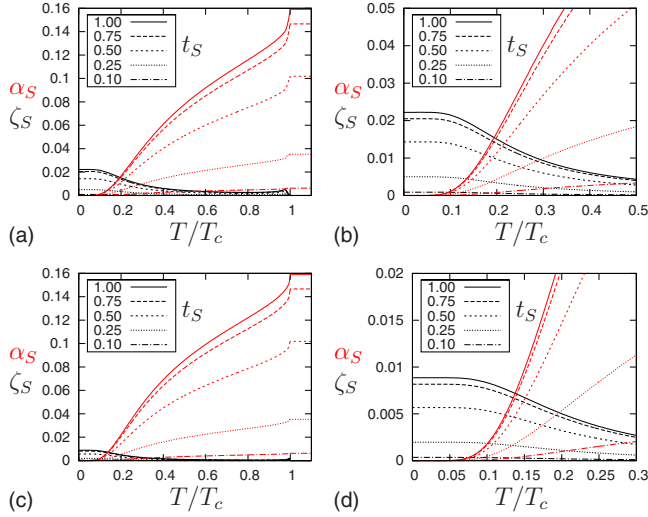
FIG. 12. (Color online) Case of a π junction ($t_S > t_0 = 0$ and $\phi = \pi$): absolute value of the Gilbert damping constant, α_S, and the shift of the precession frequency, ζ_S, as a function of temperature T for $\theta = \pi/4$. The different line styles refer to different transparencies, t_S, see the insets. The four panels correspond to (a) $h_z = 0.25\Delta$, (b) zoom on (a), (c) $h_z = 0.1\Delta$, and (d) zoom on (c).

For completeness, a similar plot for a 0 junction is shown in Fig. 13. In these figures $h_z = 0.25$ but $t_S < t_0 = 1$ in Figs. 13(a) and 13(b) whereas $t_S < t_0 = 0.75$ in Figs. 13(c) and 13(d). Provided that tunneling across the impurity still takes place, i.e., $t_S \neq 0$, these figures show the same tendency as Fig. 12 for the damping to be strongly suppressed below $T \approx 0.1 T_c$ in favor of a shift of the precession frequency due to the superconducting spin current. The magnitudes of the constants are however reduced by an order of magnitude upon reducing t_0.
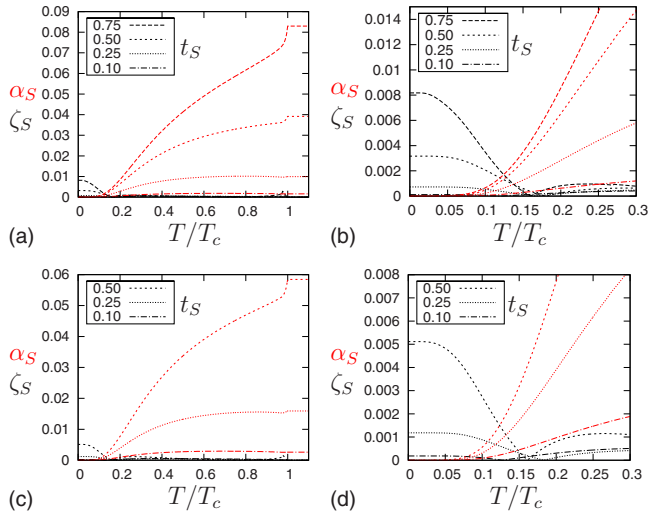

FIG. 13. (Color online) Case of a 0 junction ($t_S < t_0$ and $\varphi = 0$): absolute value of the Gilbert damping constant, α_S, and the shift of the precession frequency, ζ_S, as a function of temperature T for fixed $\theta = \pi/4$ and $h_z = 0.25\Delta$. The different line styles refer to different transparencies, t_S, see the insets. The four panels correspond to (a) $t_S < t_0 = 1$, (b) zoom on (a), (c) $t_S < t_0 = 0.75$, and (d) zoom on (c).

For a junction of arbitrary transparency, we therefore arrive at the conclusion that, deep in the superconducting phase, the precession of the spin is maintained though the frequency may be slightly lowered, in the adiabatic regime, by the condensate spin current. Other nondissipative effects, such as a nutation[35] of the localized spin due to the singlet nature of the current carriers, may then affect the motion of the molecular precessing spin but they will not suppress the magnetization dynamics.

VII. CONCLUSION

In conclusion we have presented a theory of charge and spin transport in a S/SMM/S junction where the single-molecule magnet is precessing at the frequency Ω. The theory is based on a usual Green's-function approach combined with a unitary transformation which replaces the time-dependent problem by a static one with noncolinear magnetization. Starting from the tunnel limit at zero temperature, both analytical and numerical results were presented, in a complementary way, for a junction of arbitrary transparency and at finite temperatures. Our goals were to study the out-of-equilibrium effects of the magnetization dynamics on the current flowing through the junction as well as the backaction of this current on the magnetization dynamics.

For a phase-biased junction, the unitary transformation to the rotating frame has revealed that a steady-state superconducting charge current flows through the junction and that an out-of-equilibrium circularly polarized spin current, of frequency Ω, is emitted in the leads. These currents and the corresponding CPRs were then derived and the nature of the current-carrying states was discussed. We have shown that the dynamics of the molecular spin in the junction affects both the spectrum of the Andreev states and their occupation. At high precession frequencies, it eventually leads to their disappearance as current-carrying states in favor of extended (quasiparticlelike) states. At low-precession frequencies, in particular, in the experimentally reachable adiabatic limit where $\Omega \ll 2\Delta$, and for high transparencies of the junction, the abrupt change in the occupation of the Andreev states is seen as sharp steps in the CPRs with significant variations in the current. When the transmission amplitude through the magnetic impurity dominates the direct transmission amplitude ($t_S \gg t_0$) and the junction is in a π state, the CPRs (both for charge and spin currents) show that the current is strongly suppressed around $\varphi \approx 0$ and 2π. In the opposite case of a 0 junction, still with a nonzero transmission amplitude through the magnetic channel ($t_0 > t_S \neq 0$), a similar suppression takes place around $\varphi \approx \pi$, though the magnitude of the effect is much smaller. Integrating this contact into a superconducting loop, one may hope that such sharp features could be observed experimentally. In particular, our results for the charge CPR of a π junction with a high transmission amplitude in the magnetic channel bear some similarity to experimental results on microwave irradiated SNS 0 junctions. The CPR was recently measured[44] in such a setup and the current was shown to be strongly suppressed near $\varphi \approx \pi$ upon increasing the rf power.

We have also shown that the spin current has a weak backaction on the dynamics of the magnetization deep in the

superconducting phase, i.e., at temperatures lower than the critical superconducting temperature by an order of magnitude or more. The reason is the strong suppression of quasiparticles well below T_c and in the adiabatic regime where $\Omega \ll 2\Delta$. This agrees with recent experiments on S/F hybrids[14] under FMR where the Gilbert damping was shown to be much reduced contrary to the case of N/F hybrids.[13] We have also shown that the strong suppression of the damping, at low T, goes along with a shift of the precession frequency due to the backaction of the remaining superconducting part of the spin current on the molecular magnet. The fact that the dynamics of the magnetization is only weakly affected by the backaction of the current provides a self-consistent check for the validity of the above results concerning the CPR.

[1] P. M. Tedrow and R. Meservey, Phys. Rev. Lett. **26**, 192 (1971); Phys. Rev. B **7**, 318 (1973).

[2] M. Jullière, Phys. Lett. A **54**, 225 (1975).

[3] M. Johnson and R. H. Silsbee, Phys. Rev. Lett. **55**, 1790 (1985).

[4] M. N. Baibich, J. M. Broto, A. Fert, F. Nguyen Van Dau, F. Petroff, P. Etienne, G. Creuzet, A. Friederich, and J. Chazelas, Phys. Rev. Lett. **61**, 2472 (1988).

[5] G. Binasch, P. Grünberg, F. Saurenbach, and W. Zinn, Phys. Rev. B **39**, 4828 (1989).

[6] S. A. Wolf, D. D. Awschalom, R. A. Buhrman, J. M. Daughton, S. von Molnár, M. L. Roukes, A. Y. Chtchelkanova, and D. M. Treger, Science **294**, 1488 (2001).

[7] J. C. Slonczewski, J. Magn. Magn. Mater. **159**, L1 (1996).

[8] L. Berger, Phys. Rev. B **54**, 9353 (1996).

[9] D. C. Ralph and M. D. Stiles, J. Magn. Magn. Mater. **320**, 1190 (2008).

[10] Y. Tserkovnyak, A. Brataas, G. E. W. Bauer, and B. I. Halperin, Rev. Mod. Phys. **77**, 1375 (2005).

[11] Y. Tserkovnyak, A. Brataas, and G. E. W. Bauer, Phys. Rev. Lett. **88**, 117601 (2002).

[12] X. Waintal and P. W. Brouwer, Phys. Rev. Lett. **91**, 247201 (2003).

[13] S. Mizukami, Y. Ando, and T. Miyazaki, J. Magn. Magn. Mater. **226-230**, 1640 (2001).

[14] C. Bell, S. Milikisyants, M. Huber, and J. Aarts, Phys. Rev. Lett. **100**, 047002 (2008).

[15] J. P. Morten, A. Brataas, G. E. W. Bauer, W. Belzig, and Y. Tserkovnyak, EPL **84**, 57008 (2008).

[16] C. Le Gall, L. Besombes, H. Boukari, R. Kolodka, J. Cibert, and H. Mariette, Phys. Rev. Lett. **102**, 127402 (2009); M. Goryca, T. Kazimierczuk, M. Nawrocki, A. Golnik, J. A. Gaj, P. Kossacki, P. Wojnar, and G. Karczewski, *ibid.* **103**, 087401 (2009).

[17] M.-H. Jo, J. E. Grose, K. Baheti, M. M. Deshmukh, J. J. Sokol, E. M. Rumberger, D. N. Hendrickson, J. R. Long, H. Park, and D. C. Ralph, Nano Lett. **6**, 2014 (2006).

[18] H. B. Heersche, Z. de Groot, J. A. Folk, H. S. J. van der Zant, C. Romeike, M. R. Wegewijs, L. Zobbi, D. Barreca, E. Tondello, and A. Cornia, Phys. Rev. Lett. **96** 206801 (2006).

[19] S. Sanvito and A. R. Rocha, J. Comput. Theor. Nanosci. **3**, 624 (2006).

[20] L. Bogani and W. Wernsdorfer, Nature Mater. **7**, 179 (2008).

[21] Y.-J. Doh, J. A. van Dam, A. L. Roest, E. P. A. M. Bakkers, L. P. Kouwenhoven, and S. De Franceschi, Science **309**, 272 (2005).

[22] J. P. Cleuziou, W. Wernsdorfer, V. Bouchiat, T. Ondarçuhu, and M. Monthioux, Nat. Nanotechnol. **1**, 53 (2006).

[23] P. Jarillo-Herrero, J. A. van Dam, and L. P. Kouwenhoven, Nature (London) **439**, 953 (2006).

[24] H. I. Jørgensen, K. Grove-Rasmussen, T. Novotný, K. Flensberg, and P. E. Lindelof, Phys. Rev. Lett. **96**, 207003 (2006).

[25] H. I. Jørgensen, T. Novotný, K. Grove-Rasmussen, K. Flensberg, and P. E. Lindelof, Nano Lett. **7**, 2441 (2007).

[26] C. B. Winkelmann, N. Roch, W. Wernsdorfer, V. Bouchiat, and F. Balestro, Nat. Phys. **5**, 876 (2009).

[27] A. Y. Kasumov, K. Tsukagoshi, M. Kawamura, T. Kobayashi, Y. Aoyagi, K. Senba, T. Kodama, H. Nishikawa, I. Ikemoto, K. Kikuchi, V. T. Volkov, Yu. A. Kasumov, R. Deblock, S. Guéron, and H. Bouchiat, Phys. Rev. B **72**, 033414 (2005).

[28] J. Appelbaum, Phys. Rev. Lett. **17**, 91 (1966).

[29] P. W. Anderson, Phys. Rev. Lett. **17**, 95 (1966).

[30] I. O. Kulik, Zh. Eksp. Teor. Fiz. **49**, 1211 (1965) [Sov. Phys. JETP **22**, 841 (1966)].

[31] L. N. Bulaevskii, V. V. Kuzii, and A. A. Sobyanin, Zh. Eksp. Teor. Fiz **25**, 314 (1977) [JETP Lett. **25**, 290 (1977)].

[32] J. C. Cuevas and M. Fogelström, Phys. Rev. B **64**, 104502 (2001).

[33] C. Benjamin, T. Jonckheere, A. Zazunov, and T. Martin, Eur. Phys. J. B **57**, 279 (2007).

[34] J.-X. Zhu and A. V. Balatsky, Phys. Rev. B **67**, 174505 (2003).

[35] J.-X. Zhu, Z. Nussinov, A. Shnirman, and A. V. Balatsky, Phys. Rev. Lett. **92**, 107001 (2004).

[36] J. Michelsen, V. S. Shumeiko, and G. Wendin, Phys. Rev. B **77**, 184506 (2008).

[37] S. Teber, C. Holmqvist, M. Houzet, D. Feinberg, and M. Fogelström, Physica B **404**, 527 (2009).

[38] C. Holmqvist, S. Teber, M. Houzet, D. Feinberg, and M. Fogelström, J. Phys.: Conf. Ser. **150**, 022027 (2009).

[39] R. Mélin, Europhys. Lett. **51**, 202 (2000).

[40] Using a similar approach, the Josephson current through a ferromagnet under FMR was studied in Ref. 41.

[41] M. Houzet, Phys. Rev. Lett. **101**, 057009 (2008).

[42] I. O. Kulik, Zh. Eksp. Teor. Fiz. **57**, 1745 (1969) [Sov. Phys. JETP **30**, 944 (1969)].

[43] A. A. Golubov, M. Yu. Kupriyanov, and E. Il'ichev, Rev. Mod. Phys. **76**, 411 (2004).

[44] M. Fuechsle, J. Bentner, D. A. Ryndyk, M. Reinwald, W. Wegscheider, and C. Strunk, Phys. Rev. Lett. **102**, 127001 (2009).

[45] F. Chiodi, M. Aprili, and B. Reulet, Phys. Rev. Lett. **103**, 177002 (2009).

[46] P. Virtanen, T. Heikkilä, F. Sebastian Bergeret, and J. Cuevas, arXiv:1001.5149 (unpublished).

[47] G. D. Mahan, *Many-Particle Physics* (Plenum Press, New York, 1990).

[48] Such an integral also appears in the theory of a superconductor in an alternating magnetic field, see Ref. 49.

[49] A. A. Abrikosov, L. P. Gorkov, and I. E. Dzyaloshinski, *Methods of Quantum Field Theory in Statistical Physics* (Dover, New York, 1975).

[50] A nonanalyticity of similar nature has been found in Ref. 51 where the Josephson current is a nonanalytic function of the length of the normal disordered region of an SNS junction.

[51] A. Levchenko, A. Kamenev, and L. Glazman, Phys. Rev. B **74**, 212509 (2006).

[52] The spin current, e.g., at the right lead, is defined as $\mathbf{I}^s(t) = \langle \dot{\mathbf{S}}(t) \rangle$. In the Heisenberg picture, $\dot{\mathbf{S}} = \frac{i}{\hbar}[H, \mathbf{S}]$, where $\mathbf{S}(t) = \frac{\hbar}{2} \Sigma_{\mathbf{k},\sigma,\sigma'} c_{R,\mathbf{k},\sigma}^\dagger(t) \vec{\sigma}_{\sigma,\sigma'} c_{R,\mathbf{k},\sigma'}(t)$. Upon computing the average, we go to the interaction representation and perform an expansion to the lowest meaningful order in H_T. This yields Eq. (20).

[53] B. Wang, J. Wang, and H. Guo, Phys. Rev. B **67**, 092408 (2003).

[54] At the hamiltonian level, the unitary transformation is implemented with the help of a time- and spin-dependent unitary operator, $U_{\alpha,\mathbf{k},\sigma}(t) = e^{-i\sigma\Omega t/2 c_{\alpha,\mathbf{k},\sigma}^\dagger c_{\alpha,\mathbf{k},\sigma}}$ acting on the fermionic operators of the leads, $\tilde{c}_{\alpha,\mathbf{k},\sigma}^\dagger = e^{-i\sigma\Omega t/2} c_{\alpha,\mathbf{k},\sigma}^\dagger = U_{\alpha,\mathbf{k},\sigma}^\dagger(t) c_{\alpha,\sigma}^\dagger U_{\alpha,\mathbf{k},\sigma}(t)$. The final hamiltonian then reads $\widetilde{H} = H_R + H_L + H_T(\Omega=0) - \Sigma_{\alpha,\mathbf{k},\sigma} \sigma h_z c_{\alpha,\mathbf{k},\sigma}^\dagger c_{\alpha,\mathbf{k},\sigma}$ which is equivalent to the gauge transformed action of Eq. (42).

[55] J. Rammer and H. Smith, Rev. Mod. Phys. **58**, 323 (1986); A. Kamenev and A. Levchenko, Adv. Phys. **58**, 197 (2009).

[56] C. Caroli, R. Combescot, P. Nozières, and D. Saint-James, J. Phys. C **4**, 916 (1971).

[57] J. C. Cuevas, A. Martín-Rodero, and A. Levy Yeyati, Phys. Rev. B **54**, 7366 (1996).

[58] In SNS junctions, with a normal junction of length L, extended and localized states will generally both carry the current. A "universal" regime is reached in the limit of a small junction, $L \ll \xi$, where ξ is the superconducting coherent length, where only the bound state carries the current, see Ref. 59. In the present out-of-equilibrium problem, though we consider a small junction, this statement does not hold.

[59] C. W. J. Beenakker, Phys. Rev. Lett. **67**, 3836 (1991).

[60] S. B. Kaplan, C. C. Chi, D. N. Langenberg, J. J. Chang, S. Jafarey, and D. J. Scalapino, Phys. Rev. B **14**, 4854 (1976).